

Mesendoderm Extension and Mantle Closure in *Xenopus laevis* Gastrulation: Combined Roles for Integrin $\alpha_5\beta_1$, Fibronectin, and Tissue Geometry

Lance A. Davidson,* Benjamin G. Hoffstrom,* Raymond Keller,†
and Douglas W. DeSimone*¹

*Department of Cell Biology, School of Medicine, University of Virginia Health System, Charlottesville, Virginia 22908; and †Department of Biology, University of Virginia, Charlottesville, Virginia 22903

We describe mesendoderm morphogenesis during gastrulation in the frog *Xenopus laevis* and investigate the mechanics of these movements with tissue explants. When a dorsal marginal zone explant is plated onto fibronectin, the mesendoderm moves away from the dorsal axial tissues as an intact sheet. Mesendodermal cells within these explants display monopolar protrusive activity and radially intercalate during explant extension. Live time-lapse confocal sequences of actin dynamics at the margin of these extending explants prompt us to propose that integrin-mediated traction drives these movements. We demonstrate that integrin $\alpha_5\beta_1$ recognition of the synergy site located within the type III₉ repeat of fibronectin is required for mesendoderm extension. Normal mesendoderm morphogenesis occurs with a unique “cup-shaped” geometry of the extending mesendodermal mantle and coincides with a higher rate of tissue extension than that seen in the simpler dorsal marginal zone explant. These higher rates can be reconstituted with “in-the-round” configurations of several explants. We propose several mechanically based hypotheses to explain both the initial fibronectin-dependent extension of the mesendoderm and additional requirement of tissue geometry during the high-velocity closure of the mesendodermal mantle. © 2002 Elsevier Science (USA)

Key Words: mesendoderm; integrin; fibronectin; cell migration; radial intercalation.

INTRODUCTION

During gastrulation in vertebrates, head mesoderm and ventral mesendoderm move great distances and come to lie between the ventral ectoderm and the ventral endoderm. Further elaboration of ventral organs, such as the heart, liver, kidney, and blood, depend on the success of these movements. Failure of mesendoderm morphogenesis results in severe, and frequently lethal, embryonic phenotypes. In the frog *Xenopus laevis*, these movements also result in the enclosure of the blastocoel and the isolation of the blastocoel from the ventral ectoderm. Fate mapping and lineage analysis have identified where the mesendoderm originates, when it begins to move, and the tissues to which it contributes (Bauer *et al.*, 1994; Keller and Tibbetts, 1989; Nakatsuji, 1975; Nakatsuji and Johnson, 1982; Nieuwkoop

and Florschütz, 1950; Vodicka and Gerhart, 1995; Winklbauer *et al.*, 1996; Winklbauer and Schurfeld, 1999; Lane and Sheets, 2000) (see a summary in Fig. 1A, light orange mesendoderm; after Keller, 1991 and Keller and Tibbetts, 1989). However, the mechanism driving vertebrate mesendoderm morphogenesis and the cell behaviors responsible for these movements are poorly understood. One of the reasons for this is that, in frog, like most vertebrates, the cell behaviors are obscured by either the overlying endoderm or ectoderm, forcing the use of static cell lineage and fate mapping to identify the bulk movements. It is also difficult to distinguish local force generating mechanisms in the mesendoderm from those acting at a distance from other tissues since mesendoderm morphogenesis occurs at the same time as a number of other gastrulation movements, including vegetal endoderm “rotation” (Winklbauer and Schurfeld, 1999), dorsal mesoderm convergent extension (Keller and Winklbauer, 1992), and ectoderm epiboly (Keller, 1978, 1980). In *Xenopus*, however, the local force

¹ To whom correspondence should be addressed. Fax: (804) 982-3912. E-mail: dwd3m@virginia.edu.

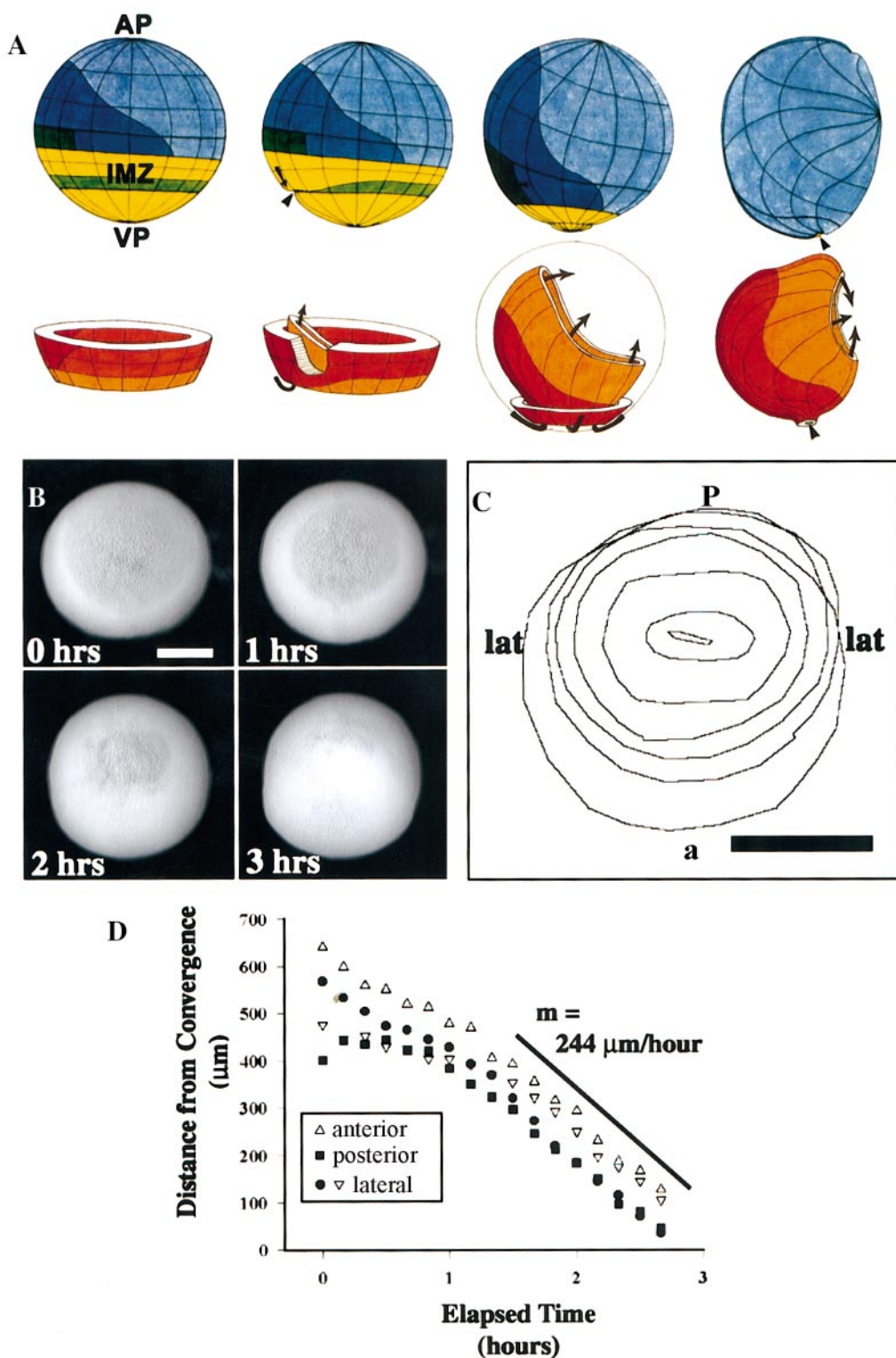


FIG. 1. Movements of the mesendoderm in whole embryos. (A) Fate map (after Keller, 1991) of the early gastrula-stage embryo. The upper set of four stages depict the fate of the superficial layer of the involuting marginal zone (IMZ; yellow and green), the neurectoderm (dark blue), and the ectoderm (light blue). The lower set of stages represent the fate map of internal tissues of the dorsal axial mesoderm (somites and notochord; red), mesendoderm (light orange), and mesoderm (orange). Bulk movements (shown by arrows) of the mesendoderm leading

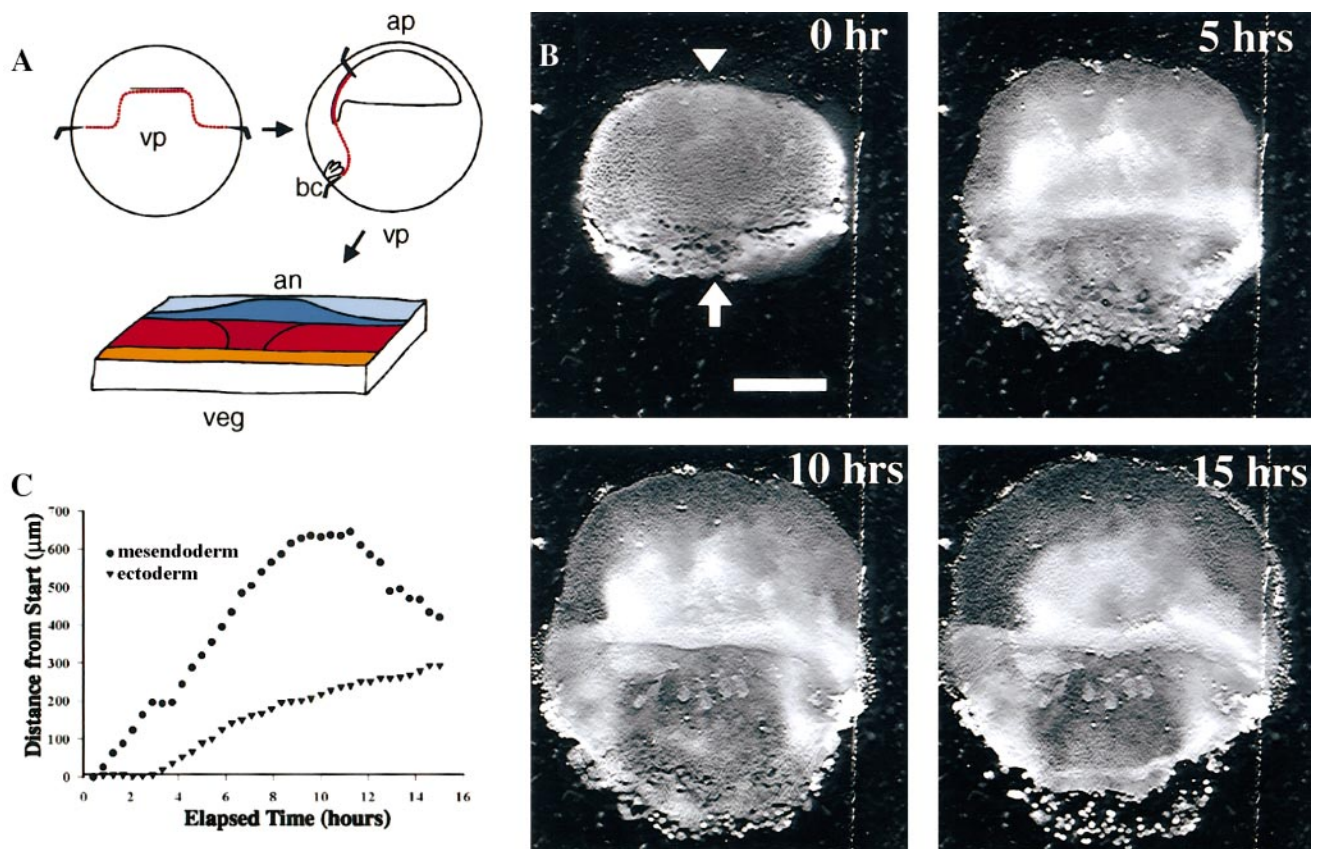


FIG. 2. Movements of the mesendoderm in dorsal marginal zone explants. (A) A schematic of how the DMZ explant is prepared. Incisions are first made at $\pm 90^\circ$ from the midline, and the vegetal mass (vegetal pole, vp) is removed. Another set of incisions is made just below the bottle cells (bc) to remove the marginal zone from the “large-cell” deep tissues and midway to the animal pole (ap). A fate map of the flattened excised tissue is drawn with the animal-vegetal axis shown (an to veg): subblastoporal endoderm (orange), notochord (central red), somite (lateral red), neural (dark blue), and epidermis (light blue). (B) Frames from a time-lapse sequence are shown as the mesendoderm advances in a typical DMZ explant. The explant, cut from an albino embryo that had been incubated in Nile blue sulfate, is slightly compressed under a coverslip (see Methods) with the deep cells facing the FN-coated substrate. The midline of the explant corresponds to the anterior midline of the embryo. The limit of involution roughly bisects the explant into upper and lower halves. (C) Graph of the progress of mesendodermal extension in the DMZ explant (see arrow in B for “starting position”). For comparison, the outward spreading of the ectoderm is also shown (see arrowhead in B for “starting position”). Scale bars indicate 500 μm .

generating tissues can be isolated and cell behaviors within them resolved by using a combination of microsurgery, molecular manipulation, and digital imaging techniques.

In view of the observation that the prospective anterior leading edge of the mesendoderm comes into contact with

fibronectin fibrils on the roof of the blastocoel (Boucaut and Darribere, 1983; Darribere *et al.*, 2000; Lee *et al.*, 1984; Winklbauer and Schurfeld, 1999), research has focused on the involvement of integrin-mediated cell adhesion and cell motility on fibronectin. One approach to understand the

edge advance, enclose the blastocoel, and converge under the animal cap ectoderm (not shown). Mesendodermal mantle closure brings cells from 360° around the marginal zone into contact at a point just posterior to the cement gland. Mesendodermal tissues underlying anterior neural and the anterior limits of the head all derive from “dorsal” midline. The blastopore lip is indicated by arrowheads and the vegetal and animal poles by vp and ap. (B) A time-lapse sequence of mesendodermal advance and closure as seen through the ectoderm of a whole albino embryo lightly compressed under a glass coverslip. (C) A series of outlines of the edge of the leading edge centered on the point in the ectoderm upon which the mesendoderm closes. (D) Graph of the progress of closure by: anterior, posterior, left lateral, and right lateral tissues. The slope of the last phase of mesendodermal closure is 244 $\mu\text{m}/\text{h}$. Scale bars in (A) and (B) indicate 500 μm .

role of fibronectin (FN) in mesendoderm morphogenesis and gastrulation is to introduce function-blocking antibodies or peptide mimics of FN cell-binding sites into the blastocoel of blastula-stage embryos. "Successful gastrulation" in these analyses has been equated with closure of the blastopore and differentiation of dorsal axial tissues; however, the phenotypes observed are likely to be more complex. In the urodele *Pleurodeles waltii*, injection of FN- and integrin-blocking reagents into the blastocoel is reported to stop mesoderm involution and extension (Boucaut et al., 1984a,b; Darribere et al., 1988, 1990). In contrast, injection of integrin function-blocking GRGDSP peptides into the blastocoel of the anuran *Xenopus laevis* slows but does not prevent blastopore closure, while dorsal axial tissues are reported to converge and extend (Winklbauer and Keller, 1996). Intrablastocoelic injection of a monoclonal antibody that blocks adhesion to the RGD-containing type III₁₀ repeat of FN also results in the retardation of blastopore closure (Ramos et al., 1996) and leads to defects in differentiation (Marsden and DeSimone, 2001). These data are consistent with earlier observations showing that removal of the blastocoel roof (i.e., the substrate for migration) stops neither blastopore closure nor convergent extension (Keller and Jansa, 1992).

Cell culture techniques have also been used extensively with single cells isolated from prospective mesendoderm or from activin-induced animal cap ectoderm to understand the role of FN in the motility of individual cells. Once removed from the embryo and grown on a FN substrate, dissociated cells or tissue fragments from the head mesoderm of both *Xenopus* and *Pleurodeles* are sensitive to the same reagents that produced variable effects in whole embryos. Function-blocking antibodies and GRGDSP peptides inhibit blastomere adhesion and cell migration on FN-coated substrates (Boucaut et al., 1990; Ramos et al., 1996; Winklbauer and Keller, 1996).

Both approaches, studies of single cell motility and the interpretation of phenotypes of whole embryos after reagents are injected into the blastocoel, are limited in their ability to decipher the mechanism of mesendoderm morphogenesis. One limitation of single-cell studies is that cell motility within the context of a tissue may differ significantly from the motility of a single cell in isolation. Cells in tissues interact with one another through cell-cell adhesion and coordinate motility through other local cell-cell interactions such as contact inhibition. Similarly, experiments that generate whole-embryo phenotypes are limited by their inability to reveal specific lesions on the cellular level; the global effects of some reagents obscure local effects due to specific cell-cell interactions. Thus, the relationship between results obtained from studies of single cells and those from whole embryos is unclear.

Several key questions remain concerning the mechanics of mesendoderm morphogenesis. What are the forces these cell behaviors generate and how do they move the ventral mesendoderm such large distances so quickly? To what extent is mesendoderm morphogenesis dependent on cell-

substrate traction and to what extent are the movements dependent on tissue-deforming forces acting between mesendodermal cells? How do these movements and the mechanical "context" of the embryo depend on FN/integrin interactions?

To answer some of these questions, we describe cell behaviors associated with mesendoderm movements, construct predictive models of how morphogenesis proceeds in the mesendoderm, and test these hypotheses using molecular and microsurgical tools. We analyze movements of the mesendodermal mantle in whole embryos at low magnification, which shows the general kinetics of the cellular movements involved. We call the movements of the mesendoderm "mesendoderm extension" since these tissues lengthen during gastrulation to enclose the blastocoel (note: *mesendoderm extension* should not be confused with *convergent extension* of the mesoderm). To characterize the cell behaviors responsible for these movements, we use microsurgery to create an explant where cell behaviors can be observed *in vivo* with high-resolution microscopy techniques. We describe two distinct models by which cell behaviors are converted to the forces that drive mesendoderm extension. After investigating a paradoxically low rate of tissue extension in the explant with respect to a high rate of extension seen in the whole embryo, we have identified a geometrical factor that enables the rapid phase of mesendodermal mantle closure. Finally we propose several models that predict how integrin-mediated cell-substrate adhesion and cell-cell adhesion generate and organize forces driving mesendoderm mantle extension and closure.

METHODS

Embryo Culture, Microsurgery, and Explant Culture

Embryos were obtained by standard methods (Kay and Peng, 1991) and staged according to Nieuwkoop and Faber (1967). Both pigmented and albino embryos were used. To enhance contrast in low-light fluorescence microscopy, embryos were injected with 1.5 nl of 25 mg/ml rhodamine dextran amine (RDA; Molecular Probes) at the one-cell stage. To visualize actin in explants, whole embryos were injected with 0.5 nl per embryo of Alexa 568 (Molecular Probes) conjugated actin protein at the 16-cell stage. Vitelline membranes were removed mechanically and microsurgery was carried out with hair-loops and -knives in Danilchik's For Amy (DFA) consisting of: 53 mM NaCl, 5 mM Na₂CO₃, 4.5 mM K Gluconate, 32 mM Na Gluconate, 1 mM CaCl₂, 1 mM MgSO₄, 1 g of bovine serum albumin (BSA) per 1 liter, and buffered to pH 8.3 with 1 M bicine (Sater et al., 1993). Antibiotic/antimycotic (Sigma A-9909; 0.1 U penicillin, 0.1 mg streptomycin, 0.25 μg amphotericin B per ml) was added to DFA to reduce explant contamination. After microsurgery, each explant was transferred by pipette to a dish or chamber, positioned, and gently compressed with a coverslip fragment held in place with high-vacuum silicone grease (Dow Chemical).

For marginal zone explants, embryos were selected at stage 10⁻ before the mesendodermal lip contacts the underside of the neural

anlagen (Poznanski and Keller, 1997). This event is not readily visible from the exterior staging criterion listed in Nieuwkoop and Faber (1967), and selection must be made after the embryo is "opened." After vitelline removal, two incisions were made 90 degrees from the anterior midline. Vegetal endoderm was then removed along with tissues that had undergone internal involution (Nieuwkoop and Florschütz, 1950). The explant was then trimmed along the vegetal side such that several rows of subblastoporal endoderm were left attached. Small wounds in the leading edge that occur during microsurgery or during transfer to a FN-coated dish can reduce the regularity of movements in the leading edge cells.

For "cap-less" and "donut" explants, embryos were selected at stage 11.5, when the mesendodermal "cup" was approximately 700 μm across. An incision through the multilayered epithelium was made around the equator of the embryo without injuring the underlying mesoderm. This "cap" was then lifted gently and teased off the mesendodermal mantle, taking care not to injure the leading edge. To make a "donut-explant," another incision was made to remove a contiguous "rim" of the mesendodermal mantle "cup" from the remainder of the embryo. This incision ran around the equator and extended into the blastocoel.

Integrin- and FN-Blocking Antibodies

Purified mAbs for 4B12 and 1F7 directed against the RGD and synergy site containing type III repeats of *Xenopus* FN, respectively, were generated from hybridoma ascites fluid by recombinant protein G affinity chromatography (Pharmacia LKB) as previously described and characterized (Ramos and DeSimone, 1996; Ramos *et al.*, 1996). The P8D4 mAb directed against the $\alpha_5\beta_1$ integrin was purified in a similar manner. Details regarding the preparation and characterization of P8D4 will be described elsewhere (B.G.H. and D.W.D., manuscript in preparation). Specific function-blocking activities of each purified mAb were confirmed by using cells dissociated from early gastrula-stage embryos plated onto FN. Purified mAbs were concentrated in DFA to between 5 and 25 mg/ml. mAbs were used at concentrations from 0.1 to 1 mg/ml to block FN substrates or to investigate mesendodermal extension in the dorsal marginal zone (DMZ).

Immunocytochemistry and in Situ Protocol

Actin in whole embryos and explants was fixed for immunostaining according to Kurth *et al.* (1999). Antibodies to actin (Cedarlane Laboratories, CLT9001) were used at 1:200. Whole embryos were prepared as "half-mounts" for sectioning according to Davidson and Keller (1999). Explants were processed intact on the original substrate, dehydrated, and cleared in benzyl benzoate and benzyl alcohol (BB:BA; 2:1). Optical sections were collected by using a confocal laser scan head (PCM2000; Nikon) mounted on an inverted compound microscope (Nikon). Notochord tissues in explants were immunostained with the tor70 antibody (Kushner, 1984) according to Domingo and Keller (1995). A peroxidase-conjugated goat anti-mouse IgM antibody (Jackson ImmunoResearch) was used to amplify the tor70 signal using the tyramide-fluorescein substrate of peroxidase. The fluorescence color reaction was carried out according to Davidson and Keller (1999).

RNA *in situ* hybridization was carried out on explants according to Davidson and Keller (1999) by using alkaline phosphatase and either NBT/BCIP (Promega) or magenta-phos (Biosynth) for detection. Images of *in situ* hybridizations and tor70 immunostains were

collected by using a digital color camera (Hamamatsu) mounted on a stereoscope (Olympus) equipped for epifluorescence.

Substrate Preparation

FN and recombinant substrates were prepared according to Ramos and DeSimone (1996). Briefly, glass coverslips were cleaned with dilute acid in ethanol then flamed. Human plasma FN (Roche Molecular Biochemicals) or the GST 9.11 fragment of *Xenopus* FN (Ramos and DeSimone, 1996) were prepared to 20 $\mu\text{g}/\text{ml}$ and incubated on glass or plastic petri dishes (Fisher) overnight at 4°C. The substrates were then washed with PBS and blocked with DFA (containing 1 mg/ml BSA) for 1 h prior to receiving explants.

Microscopy and Morphometric Analysis

Time-lapse sequences were collected with digital (Hamamatsu 4742, "Orca") and analog CCD cameras (Dage/MTI and Hamamatsu) mounted on compound upright, compound inverted, and stereo microscopes (Olympus and Zeiss). Image acquisition was controlled by software (Metamorph, Universal Imaging Corp. and NIH-Image, Wayne Rasband, version 1.62, <http://rsb.info.nih.gov/nih-image>). For the low-light fluorescence time-lapse sequences, a shutter (Uniblitz; Vincent Associates) or a filter wheel (Sutter Instruments) was also controlled by the software. Morphometric analysis was carried out on time-lapse sequences by using NIH-Image (custom macros written by L. Davidson). Time-lapse confocal sequences of live explants were collected from a laser scanning confocal microscope (Nikon PCM2000) with a 60 \times oil objective.

RESULTS

Mesendodermal Movements in Vivo

Static fate maps have tracked the gross tissue movements of the mesendoderm (Fig. 1A), but the specific cell behaviors responsible for these movements have not been observed directly. In time-lapse sequences of intact whole albino embryos, the fluid-filled blastocoel is visible as a "shadow" when viewed through the translucent animal cap ectoderm with incident illumination (Fig. 1B). The leading edge of the mesendoderm is visible along the perimeter of this shadow. Convergent movements of the leading edge can be seen as the shadow decreases in diameter. The mesendoderm migrates on the blastocoel-facing surface of the animal cap ectoderm and converges at a point on that surface. Because both the leading edge and the animal cap ectoderm are visible, rates of mesendoderm movement with respect to their ectodermal substrate could be measured. The movements of the margin of the mesendoderm were tracked and the rate of movement determined (Figs. 1C and 1D; 244 $\mu\text{m}/\text{h}$). In contrast to a previous study (Nakatsuji, 1975) that indicated that the ventral mesendo-

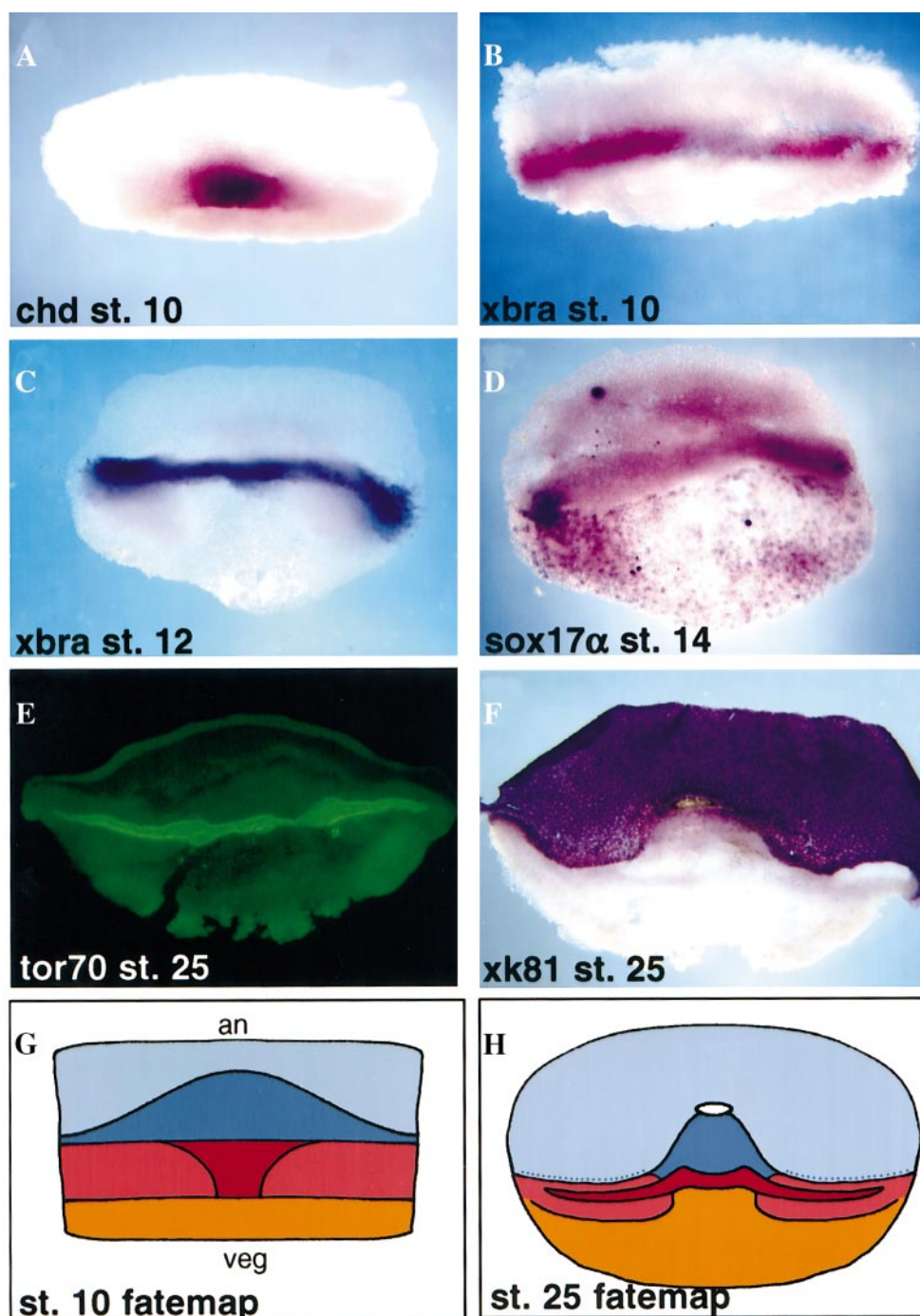


FIG. 3. Patterning of the DMZ explant parallels the intact embryo. (A) RNA *in situ* hybridization of chordin gene expression and *Xenopus* brachyury (*xbra*) gene expression (B) immediately after the DMZ explant is excised. (C) RNA *in situ* hybridization of *xbra* at stage 12 and *sox17 α* (D) at stage 14 after the mesendodermal tissues have migrated out on the FN substrate. Note that specific staining of *sox17 α* is localized to nuclei in the mesendoderm with diffuse background staining in the axial mesoderm and ectoderm. (E) Whole-mount peroxidase-amplified immunolocalization of *tor70* and RNA *in situ* hybridization of the cytokeratin gene *xk81* expression (F) identify the notochord and mesendoderm, respectively, at equivalent stage 25. A summary of the fate map is shown at stage 10 (G; the animal, *an*, to vegetal, *veg*, axis is indicated) and at stage 25 after morphogenetic movements within the DMZ explant (H). For (G) and (H), see Fig. 1A for legend.

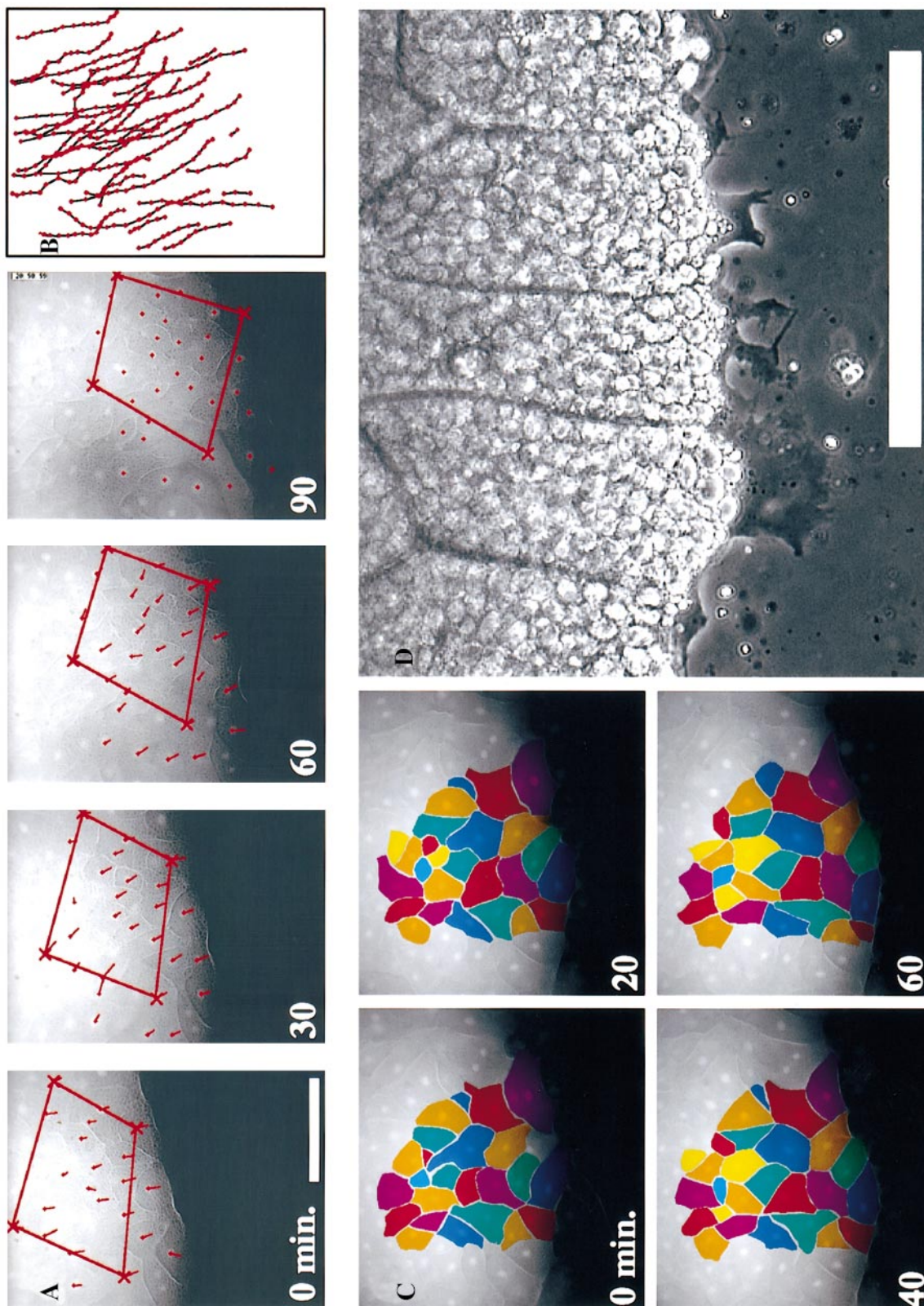


FIG. 4. Time-lapse sequences of mesendoderm extension. (A) Representative time-lapse sequence of extending mesendoderm in which individual nuclei are tracked (red crosses) over 90 min. A box drawn over a group of cells does not deform as the sheet extends but instead translocates as the sheet moves. Scale bar is 250 μm . (B) Tracks (black lines) covered by cell nuclei (red dots) at 5-min intervals over the course of the time-lapse sequence in (A). Short tracks indicate cells that arrive on the substrate during the course of the time-lapse sequence. (C) Rearrangement is rare among cells in the mesendoderm. Frames at 20-min intervals from a time-lapse sequence show little cell rearrangement. A green cell that starts behind the leading edge at 0 min undercuts and takes over a position at the leading edge within 40 min. (D) Leading edge cells extend broad lamellae in the direction of mesendoderm movement. Scale bar is 100 μm .

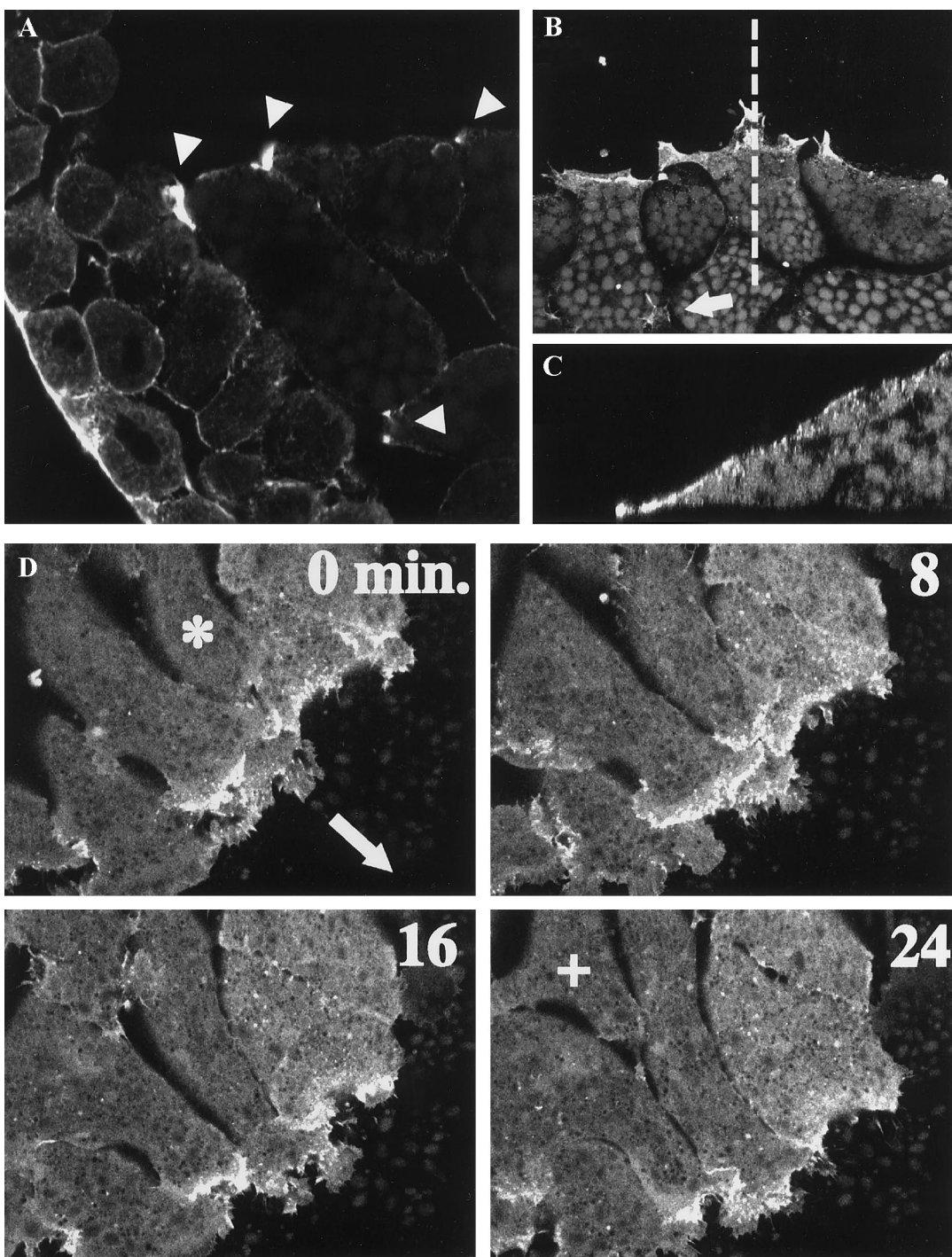


FIG. 5. Actin-rich lamellae mark the leading edge as well as cells within the mesendodermal mass of both DMZ explants and whole embryos. (A) An optical confocal section shows that actin localizes strongly to the leading edge of the mesendoderm in whole embryos. Arrowheads show intense actin localization in the leading edge as well as in cells within the mesendodermal mantle. (B) A sum of 12 confocal sections from an *en-face* view of the leading edge of a DMZ explant show strong actin localization to the leading edge. Occasional smaller lamellae are visible behind the leading edge (arrow). (C) An X-Z section taken along the dotted line in the confocal stack collected in (B). (D) Confocal time lapse of actin dynamics at the leading edge (an arrow shows the direction of mesendodermal explant extension). Several cells can be seen in frames from a 24-min-long time-lapse sequence. These cells exhibit complex actin dynamics at the leading edge: intense actin localization at cell-cell boundaries and actin within lamellae at the leading edge as well as in lamellae extended by cells within the mass of the mesendoderm. One cell (marked by "*" at 0 min) overtakes cells already on the leading edge. Another cell (marked by "+" at 24 min) extends a lamella onto the substrate behind the leading edge. Fluorophore-conjugated actin was injected into embryos at the 16-cell stage targeting the midline. Single frames were collected every 15 s from the plane of the substrate. One frame is 213 μm across.

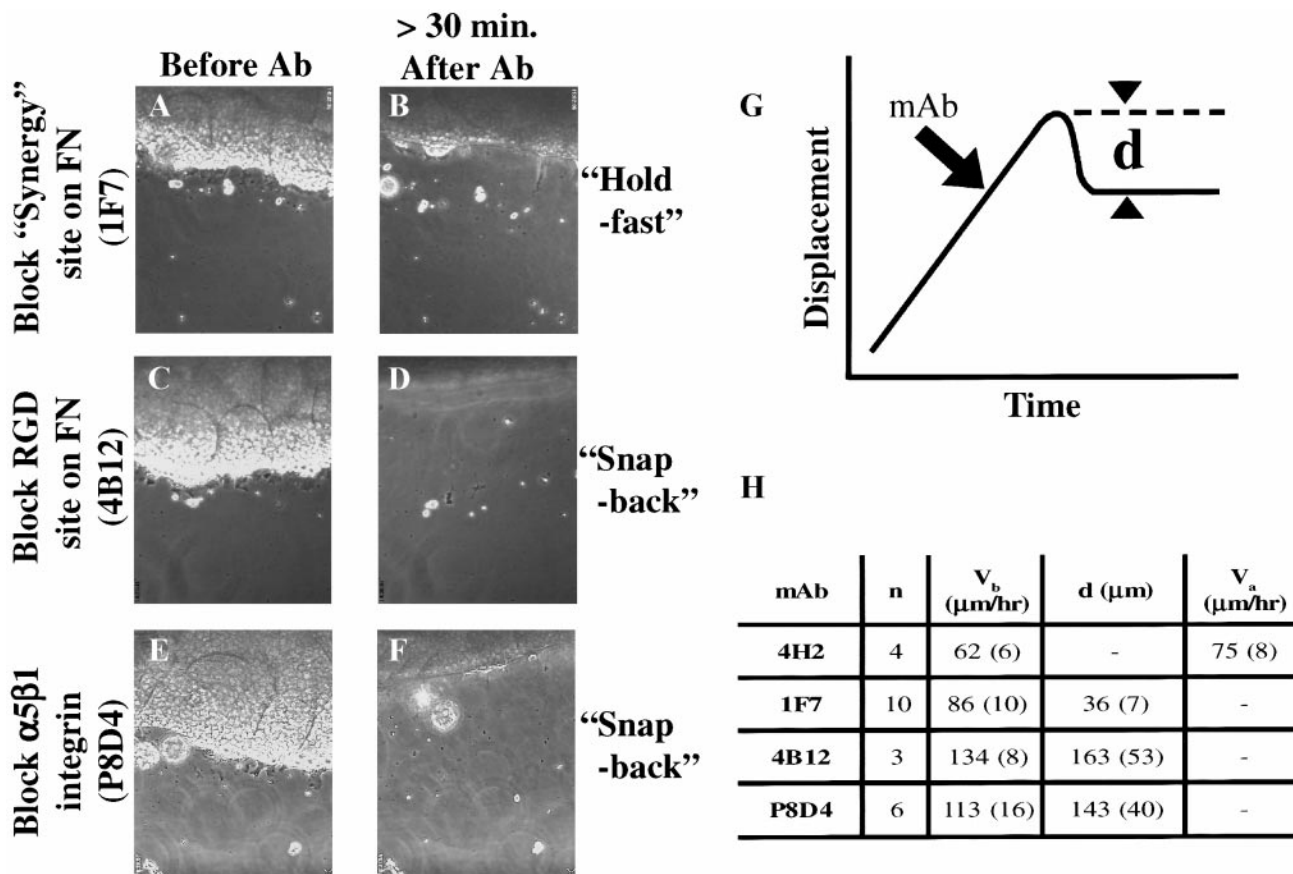


FIG. 6. Function-blocking antibodies to FN and $\alpha_5\beta_1$ integrin disrupt extension and adhesion selectively. Frames from representative video phase microscopy time lapses collected before (A, C, E) and after (B, D, F) explants were incubated with the blocking antibodies. The leading edge extends downward in each experiment. (A, B) Addition of mAb 1F7 causes the explant to reduce protrusive activity but the explant "holds-tight" onto the substrate. (C, D) Addition of mAb 4B12 causes the explant to "snap-back." (E, F) Addition of mAb P8D4 causes an extending explant to reduce protrusive activity and "snap-back" from its full extent. (G) Schematic of antibody blocking experiment. The displacement of the leading edge of the mesendodermal explant is tracked with time and antibody is added (arrow). Shortly after the antibody is added, the explant stops extending (dotted line) and retracts a distance (d). Explants can retract only one or two cell diameters, i.e., "hold-tight," or may retract more, i.e., "snap-back." (H) Table of antibody results. The velocity is measured before antibody treatment (V_b) and after (V_a) for the control antibody 4H2. The degree of retraction is measured (d) when the antibody affects explant extension. Standard error for the number of repetitions (n) is given in parentheses.

derm does not extend, we found that the posterior leading edge starts to extend later than the anterior leading edge but ultimately reaches the same rate of extension as the anterior mesendoderm. While the optically translucent cell layers of the albino animal cap ectoderm allow the identification of the leading edge mesendoderm, these tissues obscure the tracking of individual cells.

Mesendoderm Movements in an Explant of the DMZ

To resolve individual cells and their behaviors, we developed an explant from the marginal zone of early gastrula-stage embryos. This explant was made by removing the

entire dorsal half of the marginal zone from early stage-10 embryos (DMZ explant; Fig. 2A). To mimic the FN matrix of the underside of the animal cap, these explants were placed onto glass coverslips coated with FN. Like similar explants of the DMZ (Keller *et al.*, 1985), these explants consist of super- and subblastoporal endoderm, mesendoderm, mesoderm, neural, and ectodermal tissues. Shortly after these explants are placed onto an FN-coated substrate, the mesendoderm crawls out onto the substrate and away from the explant as a sheet (Fig. 2B). The rate of movement of this sheet is approximately $100 \mu\text{m/h}$ (dots in Fig. 2C). After 10 h, the rate of mesendodermal movement slows and the leading edge retracts (Figs. 2B and 2C, compare 10- and 15-h time points). Explants made with the complete mes-

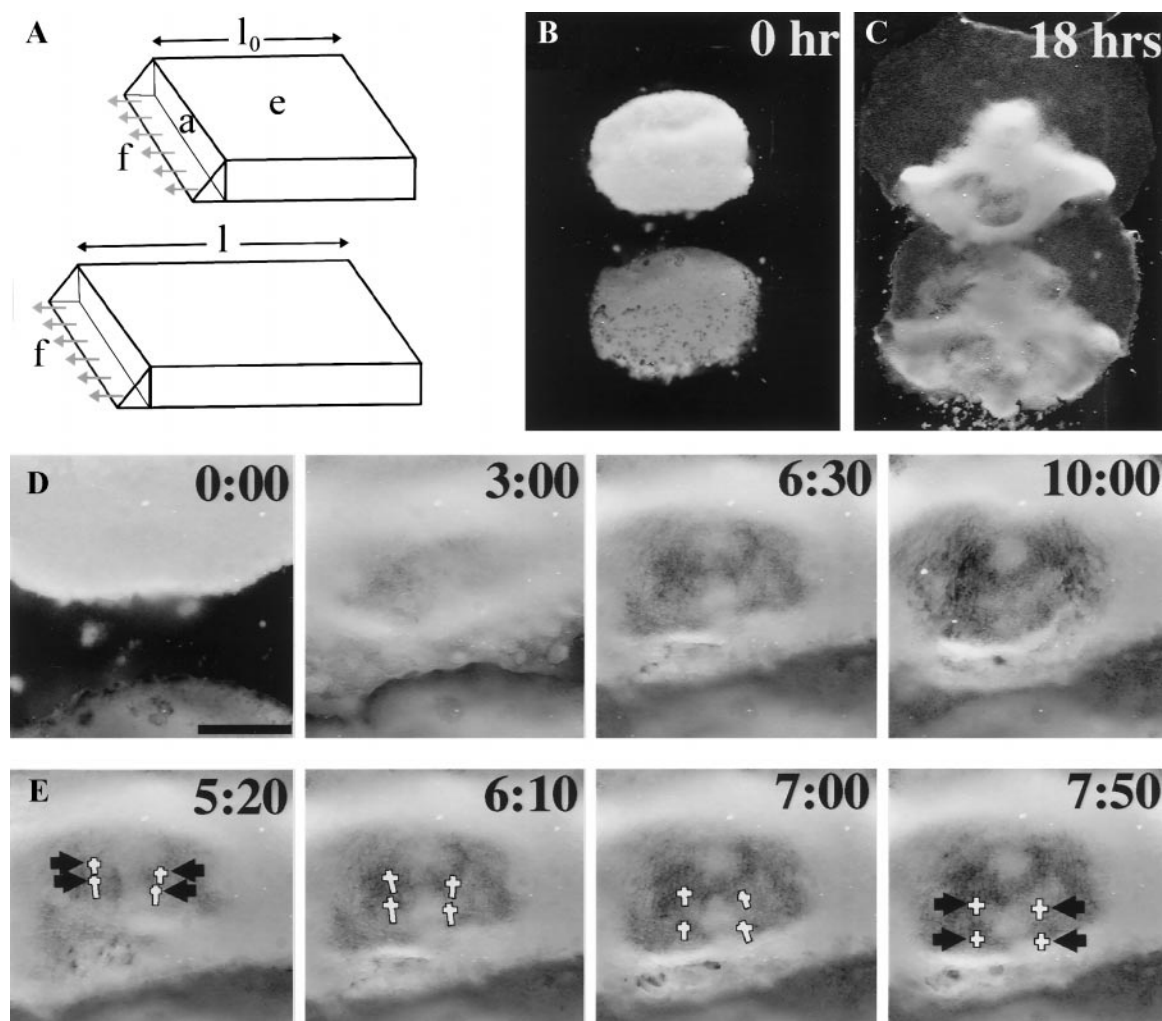


FIG. 7. The “propulsive leading edge” model for mesendoderm extension and a test of that model. (A) A schematic of the “propulsive leading edge.” The early mesendoderm consists of a leading edge generating force (f) through its area of contact with the remainder of the mesendodermal mantle (a). The mesendodermal mantle passively resists deformation with an elastic modulus (e) and stretches from an initial length (l_0). Forces generated from the leading edge pull on the mesendodermal mantle deforming it to the new length (l). In this model, forces for extension are the result of cycles of extension and contraction of protrusive lamellae along the free leading edge. (B) Two DMZ explants are placed onto an FN-coated plastic dish. Both are oriented such that the ectoderm is up, the mesendoderm is down, and the midline bisects the explant. (C) The two explants in (B) 18 h later show that a collision has occurred between the mesendodermal sheet of the upper explant and the ectoderm of the lower explant. (D) A time-lapse sequence shows collision of the two explants. (E) Additional frames from the time-lapse sequence in (D) show continuing movement of cells (see four arrows) behind the leading edge after the collision. These four cells move at an average $90 \mu\text{m}/\text{h}$ after the collision (crosses indicate where the cells start and tails are proportional to the distance moved). Scale bar for time-lapse frame in (D) indicates $500 \mu\text{m}$.

endodermal lip, i.e., including the tissue that contacts the underside of the ectoderm, display similar rates of mesendoderm migration (data not shown). The rate of mesendoderm movement is not simply a feature of any tissue placed on FN. While prospective epidermis adheres and spreads on FN, its rate of movement is limited to less than $25 \mu\text{m}/\text{h}$ (triangles in Fig. 2C), and unlike the mesendoderm, extension continues beyond 10 h.

Early Morphogenetic Movements of the Mesendoderm in the DMZ Explant Are Decoupled from the Morphogenesis of the Axial Mesoderm

We confirmed the presence of mesendoderm in our explants with an analysis of gene expression. To visualize gene expression patterns specific to the marginal zone, we carried out a battery of RNA *in situ* hybridizations (Figs.

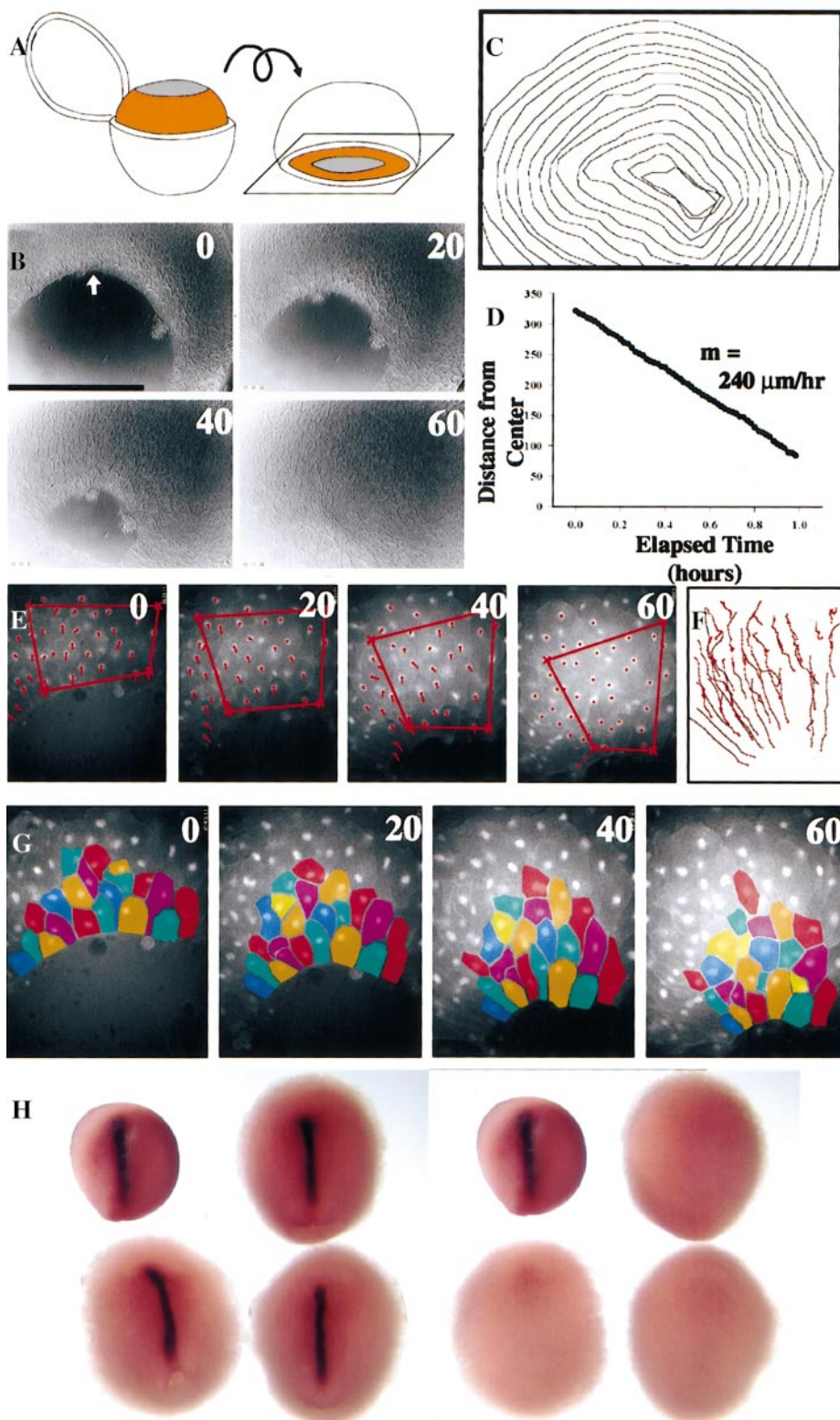


FIG. 8. High rate of mesendoderm extension proceeds in a cap-less explant. Movements of the mesendoderm in “cap-less” explant. (A) Schematic showing how cap-less explants were prepared. (B) A representative time-lapse sequence of mesendodermal advance and closure of the cap-less explant. (C) A series of outlines taken every 5 min of the edge of the leading edge centered on the point upon which the

3A–3F). These patterns revealed several interesting features of these explants. Figures 3A and 3B show the extent of the DMZ that remains in these explants following microsurgery. Explants fixed immediately after excision were stained for expression of chordin (Fig. 3A) and *xbra* (Fig. 3B). The blastoporal lip is clear at the lower boundary of chordin expression in Fig. 3A. Under the lip can be seen a small quantity of subblastoporal endoderm. Expression of *xbra* at this stage is characteristic of prospective notochord and somites. The fate map of the DMZ explant shortly after excision is summarized in Fig. 3G. After plating the explant onto FN, the mesendodermal tissues migrate out and away from the dorsal axial tissues. *Xbra* gene expression at equivalent stage 12 (Fig. 3C) shows the location of the dorsal axial tissues in the explant while *sox17 α* gene expression (Fig. 3D) indicates how far the mesendoderm has migrated by equivalent stage 14. Thus, the early morphogenetic movements of the mesendoderm in explants are mechanically isolated, decoupled from the morphogenesis of more axial mesoderm. Finally, Figs. 3E and 3F illustrate the ultimate patterning of these explants. The differentiation marker *tor70* shows the extent of notochord formation (Fig. 3E). Epidermal differentiation is indicated by sharply restricted gene expression of the cytokeratin marker *xk81*. Clearly, medial convergence of the axial mesoderm is blocked but differentiation is not (Fig. 3H). What is clear from these gene expression patterns is that the mesendoderm in the DMZ explant extends perpendicular to the axial mesoderm, mimicking the normal movement in whole embryos, where head, lateral, and posterior mesendoderm move away from the dorsal axis (Fig. 1A).

Extension of DMZ Mesendoderm Explant Is Coincident with Radial Intercalation within the Sheet and Protrusive Activity at the Leading Edge

We observed that movement of the mesendoderm in the DMZ explant occurs in the absence of mediolateral intercalation of mesendoderm cells (Fig. 4A). A box drawn around a typical group of mesendoderm cells does not deform as predicted for convergent extension (i.e., lengthen and narrow, cf. Keller and Tibbetts, 1989) but instead appears to translocate *en masse*. Tracks of individual cell nuclei within the sheet move in the same direction as the extending sheet (Fig. 4B). Extension of the mesendoderm is

accompanied by only a small degree of neighbor exchange (Fig. 4C) consistent with previous work (Keller and Tibbetts, 1989).

The tissue architecture of the mesendodermal sheet in these explants mimics the architecture of the mesendodermal mantle in whole embryos. When the explant is placed onto an FN-coated substrate, a single layer of cells contact and adhere to the substrate. Explants typically begin with multiple layers of cells. As the mesendoderm migrates out from the axial mesoderm, it thins from multiple layers of cells occasionally becoming only one-cell layer thick. The cells in direct contact with the FN substrate become “shingled” just as cells within the whole embryo (Fig. 5A; Winklbauer *et al.*, 1991). Cells in deeper layers join those cells already on the FN substrate through the process of radial intercalation. Radial intercalation occurs at the leading edge and throughout the mesendodermal mantle, even as the tissue moves forward. Radial intercalation is seen as cells from deeper layers send out protrusions between cells that are already contacting the substrate. Within a few minutes, these deep-originating cells intercalate, attach to the substrate, and begin moving in the same direction as their neighboring cells (see Fig. 11D; see time-lapse sequence shown in Fig. 4 online at <http://www.dbtimelapses.org/timelapses.html>). Intercalating cells frequently appear on the FN substrate next to cells that had intercalated earlier, as if taking advantage of openings or weak locations in the cohesive cell mass (e.g., yellow cells in Fig. 4C).

Time-lapse sequences show that cells occasionally join the leading edge (e.g., Fig. 5D) and, like their neighbors, exhibit extensive arrays of cellular protrusions (Fig. 4D). Similar to migrating isolated mesoderm cells in culture (Selchow and Winklbauer, 1997), the leading edge cells in the DMZ explant extend large dynamic lamellae in the direction of movement. *Xenopus* mesendoderm cells are extremely yolk granule laden. Lamellae are yolk-free, readily observed by phase microscopy, and often extend up to 30 μm from the cell body. Nearly all the cells on the leading edge extend lamellae (Figs. 4D and 5D); those that do not are either in the process of cell division or in the process of being removed or passed by actively protruding neighbor cells. Even though these cells are mesenchymal and not epithelial in nature, we have never observed cells detaching from their neighbors and migrating off the leading edge.

mesendoderm converges. (D) Graph of the progress of closure in the cap-less explant (indicated by arrow in B). The velocity of the mesendoderm, 240 $\mu\text{m}/\text{h}$, is shown as the slope of the trace. Scale bar in (B) indicates 500 μm . (E) A representative time lapse of mantle closure in the cap-less explant. Individual nuclei are tracked over 60 min. A bounding box deforms as the mantle closes but cells within tissue are translocating rather than mediolaterally intercalating (F). (G) Cell rearrangement occurs as the edge of the mantle converges, reducing the number of cells along the margin from 12 to 6. Radial intercalation brings three new cells onto the substrate. (H) Axial mesoderm shown by the expression of the notochord-specific gene chordin is present on the dorsal surface (three explants; left panel) but not seen on the ventral surface (right panel) where mantle closure occurs. The dorsal side of an equivalent stage-14 embryo is shown in the upper left of both panels.

Actin Organization in the DMZ Explant Parallels Actin Cytoskeleton in the Whole Embryo

Tissue movements and patterning in DMZ explants appear to reflect events in whole embryos; however, we do not know whether the subcellular distribution of specific molecular components of the DMZ explant parallel those observed in the whole embryo. To resolve this question, we investigated the localization of actin in both DMZ explants and whole embryos.

There is striking similarity between actin localization in the whole embryo (Fig. 5A) and the DMZ explant (Figs. 5B and 5C). Actin is strongly localized to the leading edge in both the DMZ explant (Fig. 5B) and the mesendodermal mantle *in vivo* (Fig. 5A). Actin can also be found behind the leading edge *in vivo* as well as in the DMZ explant (arrowheads in Fig. 5A and arrow in Fig. 5B), perhaps marking cells in the process of radial intercalation. Several differences between the DMZ explant and the whole embryo can also be observed. While the leading edge in whole embryos develops discrete actin-rich structures in the direction of mesendoderm movement, the long lamellae present in the explant are not observed in the whole embryo (Fig. 5C vs. Fig. 5A). This absence may reflect the difference between an FN substrate on a glass scaffold and the FN fibrils found on the deformable scaffold of the animal cap ectoderm. The absence of long actin-rich lamellae in the whole embryo may also reflect a fixation artifact due to the difficulty of simultaneously preserving actin and lamellae.

Since actin fixation has many known disadvantages, we injected a fluorescently coupled actin into early cleavage-stage embryos and followed actin dynamics in live DMZ explants (Fig. 5D; see time-lapse sequences of actin dynamics online at <http://www.dbtimelapses.org/timelapses.html>). Confocal time-lapse sequences of actin dynamics in the leading edge support the observations of actin in the fixed samples. Actin localizes to the dynamic lamellae seen in phase contrast. Actin can also be seen at cell-cell boundaries but appears more intense just behind advancing cell margins. Two cells in the sequence illustrate the role of actin in the process of radial intercalation and the addition of a cell to the leading edge, respectively.

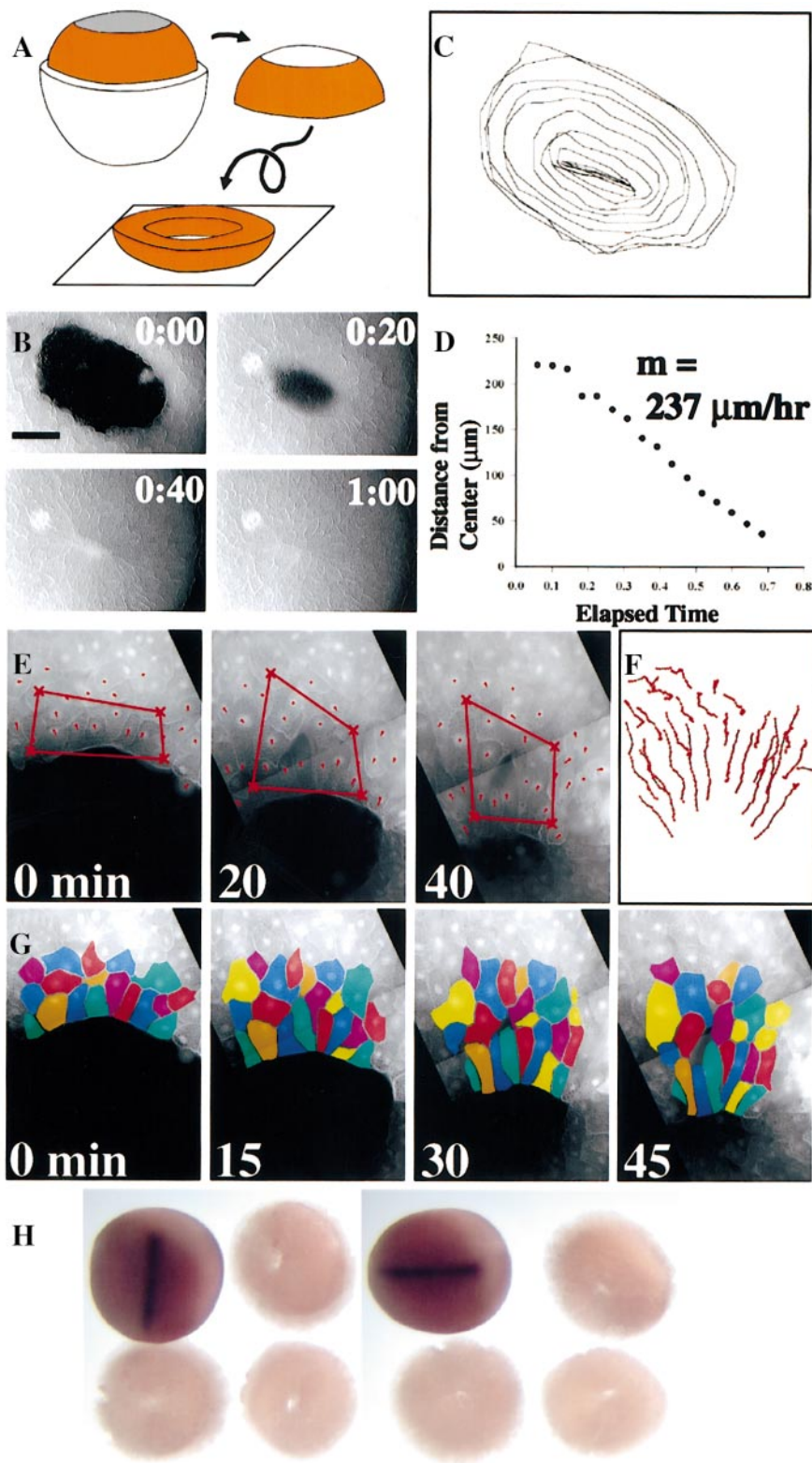
Actin dynamics in the explant differ significantly from fixed actin seen in isolated cells. Previous workers have

observed actin localization in fixed isolated mesendoderm (Selchow and Winklbauer, 1997) and activin-induced animal cap cells (Gurdon *et al.*, 1999) and found extensive actin localized throughout the cell with considerable actin localized to both the leading and trailing edges of migrating cells. From our observations of actin in fixed whole embryos and within live cells of the DMZ explant, we also see actin at the leading edge of cells but not at the trailing edge. Cells migrating in isolation (Winklbauer and Selchow, 1992) appear to lack the tightly regulated morphology seen in explants where cells develop a polarized, shingled shape and maintain highly persistent directed protrusive activity.

What Is the Role of Integrin/FN in Mesendoderm Extension?

Since microfilaments form extensively at the substrate level of the leading edge and integrins function as a mechanical link between the cytoskeleton and the extracellular matrix (Sastry and Horwitz, 1993), we decided to investigate the role of integrin-mediated cell-substrate adhesion in driving mesendoderm extension. The forces driving these movements may be generated by each cell that makes contact with the FN substrate. In order to test this hypothesis, we utilized antibodies capable of blocking specific cell-binding domains of *Xenopus* FN (Ramos and DeSimone, 1996). The first antibody we used, mAb 1F7, blocks cell recognition of the “synergy” site located in the type III₉ repeat of the FN molecule. This antibody has no effect on the attachment of single cells to FN but does block spreading and migration. Recently, mAb 1F7 has also been shown to block FN fibril formation in the animal cap ectoderm (Marsden and DeSimone, 2001). DMZ explants were placed onto a recombinant fragment of *Xenopus* FN (GST 9.11) that contains both the synergy and RGD sites, which represent the minimal set of binding domains necessary for cell attachment and migration in this system (Ramos and DeSimone, 1996). There is no difference in the rate of extension of mesendoderm on either GST 9.11 or human plasma FN (data not shown). The mesendoderm was then allowed to migrate out and antibody was added to the culture media (arrow in Fig. 6G). Forward movement of the DMZ explant ceases and the leading edge lamellae retract after mAb 1F7 is added, demonstrating that the “synergy”

FIG. 9. High rate of mesendoderm extension proceeds in a donut explant. (A) Schematic showing how donut explants were prepared. (B) A representative time-lapse sequence of mesendodermal advance and closure of the donut explant over the course of 1 h. This explant was cultured on a minimal substrate (GST 9.11) containing the RGD and synergy site of the central cell-binding domain of *Xenopus* FN. (C) A series of outlines taken every 5 min of the edge of the leading edge centered on the point upon which the mesendoderm converges. (D) Graph of the progress of closure in the donut explant. The velocity of the leading edge, 237 $\mu\text{m}/\text{h}$, is shown by the slope of the trace. Scale bar in (B) indicates 200 μm . (E) A representative time lapse of mantle closure in the donut explant. Individual nuclei are tracked over 40 min. A bounding box deforms as the mantle closes, but (F) cells within tissue are translocating rather than mediolaterally intercalating. (G) Cell rearrangement occurs as the edge of the mantle converges, reducing the number of cells along the margin from eight to five. Radial intercalation brings five new cells onto the substrate. (H) Axial mesoderm shown by the expression of the notochord-specific gene *chordin* is absent from both dorsal surface (three explants; left panel) and the ventral surface (right panel) where mantle closure occurs. The dorsal side of an equivalent stage-14 embryo is shown in the upper left of both panels.



site on FN is required for extension of the mesendoderm within the DMZ explant (Figs. 6A, 6B, and 6H). When an antibody known to block the RGD-containing type III₁₀ repeat sequence of FN is used (mAb 4B12), mesendodermal movement not only stops, but the already extended mesendoderm detaches and retracts (Figs. 6C, 6D, and 6H; a control nonfunction blocking antibody to FN, mAb 4H2, has no effect; Fig. 6H). Since recognition of both RGD and synergy involves the integrin $\alpha_5\beta_1$ (Danan *et al.*, 1995), we also tested an antibody that blocks the function of the $\alpha_5\beta_1$ integrin directly (mAb P8D4; B.G.H. and D.W.D., manuscript in preparation). Application of mAb P8D4 causes mesendodermal movement to stop and the already extended mesendoderm to retract from its previous position (Figs. 6E, 6F, and 6H for mAb P8D4), confirming the involvement of $\alpha_5\beta_1$ integrin. Thus, while adhesion to the FN substrate via the RGD site is a prerequisite for attachment and maintenance of the extending mesendoderm, it is the involvement of integrin $\alpha_5\beta_1$ with the “synergy” region of FN that enables mesendoderm morphogenesis in the DMZ explant.

Are the Forces That Drive Mesendoderm Extension Generated at the Leading Edge?

The presence of strong protrusive activity coupled with dynamic actin polymerization in the leading edge and the sensitivity of these protrusions to synergy-blocking antibodies prompts us to propose the “propulsive leading edge” model for mesendoderm extension (Fig. 7A). This model posits that the forces driving extension are the direct result of protrusive activity in the first row of cells along the leading edge. Studies of protrusive activity in single cells demonstrate that protrusions can generate considerable force (Dembo and Wang, 1999; Galbraith and Sheetz, 1999; Oliver *et al.*, 1994; Pelham and Wang, 1999). One prediction of this model is that if one could block protrusive activity specifically at the leading edge, then one could block extension of the entire mesendodermal sheet. However, inhibitors of the contractile actomyosin machinery involved in the generation of force at the leading edge may alter force generating mechanisms operating elsewhere in the tissue or even alter tissue stiffness. Alternatively, according to the model, physically blocking the progress of the leading edge should bring movement within the sheet to a halt.

With this testable prediction, we set out to block the progress of the leading edge in the DMZ explant by placing two explants onto FN (Fig. 7B), oriented such that the mesendoderm of one explant (upper explant in 7B) would extend and collide with the ectoderm of the other explant (lower explant in 7B). The explants collide as expected (Fig. 7C), bringing the leading edge to a halt (Fig. 7D). However, cells further back in the mesendodermal mass continue to move forward at the same rate as an unconfined explant (arrows in Fig. 7E). Thus, tissues behind the leading edge continue to move forward even when progress of the

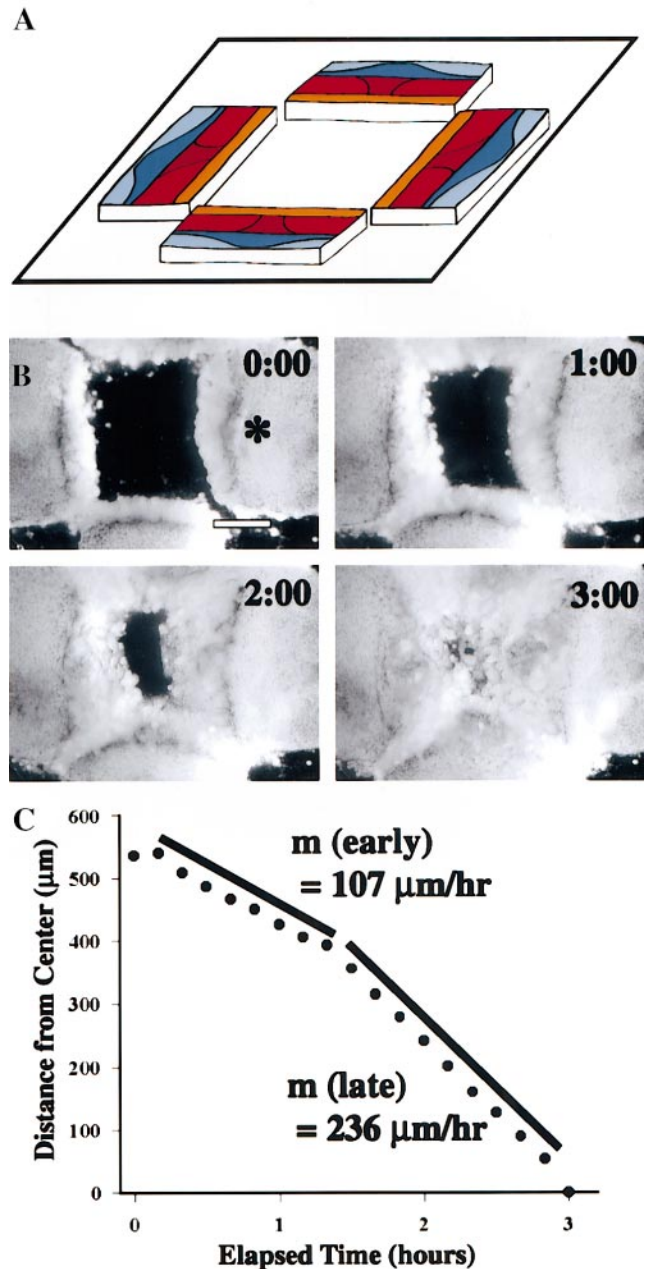


FIG. 10. “In-the-Round” arrangement restores high rate of mesendoderm extension to the DMZ explant. Movements of the mesendoderm in DMZ explants arranged in a circle. (A) Schematic showing the layout of the DMZ explants with the prospective fate of each explant shown (see Fig. 2). (B) A representative time-lapse sequence of mesendodermal extension, joining of the extending sheets, and closure over 3 h. (C) Graph of the progress of an advancing explant (asterisk in B) during the sequence shown (B). The velocity of the early and late phase of extension is shown by the slopes of the trace. Scale bar in (B) indicates 500 μm .

leading edge is physically blocked. Thus, protrusive activity of the leading edge is not solely responsible for the movement of the entire mesendodermal mantle. Alternative models for the forces driving mesendoderm extension in the DMZ explant are proposed in the discussion.

In-The-Round Geometry of the Leading Edge Is Both Necessary and Sufficient for the Increased Rate of Movement Observed in Vivo

Comparison of the rate of mesendoderm movement in the DMZ explant and movement of the leading edge *in vivo* reveals that the DMZ explant achieves only half the rate of extension seen *in vivo* (compare Figs. 1D and 2C). The rate of DMZ extension we observe is consistent with the directed migratory rate of mesendodermal tissue “slugs” cut from the DMZ (Winklbauer, 1990) and placed onto FN. This rate is also consistent with the randomly directed migratory rate of single cells dissociated from mesendoderm isolated from the DMZ (Ramos *et al.*, 1996). While explants rarely perform morphogenetic movements as well as the intact embryo, we could identify three characteristics of the DMZ explant that might limit the efficiency of cell migration. The first feature is the organization of the extracellular matrix presented to the explant. Explants can extend on a minimal substrate consisting of the GST 9.11 fragment of *Xenopus laevis* FN. In contrast, the mesendodermal mantle *in vivo* sees a milieu of complex extracellular matrix in the blastocoel, including FN fibrils, bound to the underside of the animal cap. Substrate rigidity is another contrasting factor between the environment of the DMZ explant and the intact embryo. Cultured cells can change morphology and migration rate when grown on substrates of different elastic moduli (Choquet *et al.*, 1997; Lo *et al.*, 2000). Traction exerted by cells in the DMZ explant are met with the mechanical resistance of molecular FN adsorbed onto glass. *In vivo*, the same cells attach to FN fibrils that are bound to a much more pliant substrate of the animal cap ectoderm. Finally, the linear geometry of the DMZ explant with both ends “open,” excised from lateral tissues, contrasts with the contiguous 360° perimeter of the leading edge *in vivo*. To identify which of the characteristics of the DMZ explant reduces the rate of extension, we developed several additional explants where effects of these features could be evaluated.

The simplest of these explants revealed that neither substrate complexity nor substrate mechanical properties were responsible for the increased rate of movement seen in the intact embryo. The “cap-less” explant is made from a stage-11.5 embryo that has had its animal cap ectoderm removed (Fig. 8A). This explant is then plated onto an FN-coated glass coverslip and its movements recorded in a time-lapse sequence (Fig. 8B). Analysis of these movements shows that the cap-less explant recapitulates the migratory rate of the intact embryo (Figs. 8C and 8D; $n = 8$). Thus, FN fibrils are not required for the increased rate of movement in the intact embryo.

Mesendoderm closure in the cap-less explant occurs in the absence of mediolateral intercalation. A bounding box drawn around cells in the mesendodermal mantle deforms (Fig. 8E) as the mantle closes. Cells along the leading edge converge, however, tracks of individual nuclei translocate *en masse* (Fig. 8F) just as they do in the DMZ explant. Radial intercalation is also seen as the mantle closes (see yellow cells in Fig. 8G). In contrast, with the case of the DMZ explant, cells in the closing mantle rearrange as the mantle closes. As the perimeter of the closing mantle decreases, cells leave the leading edge and join the second tier of cells (e.g., six cells leave the leading edge during the time lapse shown in Fig. 8G).

Dorsal axial tissues do not contribute directly to mantle closure in the cap-less explant. To show that the anterior end of the notochord was not driving closure of the mantle, we characterized cap-less explants immediately after closure for the expression of chordin (Fig. 8H). While the dorsal face of the explant clearly shows the location of the notochord, the ventral surface shows the complete absence of the notochord from the mesendodermal mantle.

Because the cap-less explant retains an intact blastocoel as well as the rest of the embryo and is cultured on full-length FN, we thought unknown components remaining within the blastocoel or nonintegrin cell substrate-binding sites might contribute to the high rate of movement observed. We tested this hypothesis by excising the leading edge from the cap-less explant (the “donut” explant; Fig. 9A; $n = 2$), plating the explant on the minimal fragment of FN containing a single RGD and synergy site (GST 9.11) and recording its movements in a time-lapse sequence (Fig. 9B). Remarkably, the leading edge in the donut explant (Figs. 9C and 9D) extends with a rate comparable to both the cap-less explant and the intact embryo. Both the cap-less and the donut explant retain the leading edge in a contiguous 360°.

Mesendoderm closure in the donut explant occurs without mediolateral intercalation and in the total absence of axial mesoderm. A bounding box drawn around cells in the donut explant shows limited convergence of the leading edge of cells (Fig. 9E) as the mantle closes. Like the cap-less explant, convergence appears to be driven by geometry since tracks of individual nuclei translocate *en masse* (Fig. 9F). Radial intercalation is also seen as the donut closes (see yellow cells in Fig. 9G). Like the cap-less explant, cells in the closing mantle of the donut explant rearrange as the margin of the mantle closes. As the perimeter of the mantle decreases, cells leave the leading edge and join the second tier of cells (e.g., three cells leave the leading edge during the time lapse shown in Fig. 9G). Lack of chordin expression confirms the complete absence of axial mesoderm in the donut explant (Fig. 9H). While the cap-less explant retains prospective axial mesoderm with its possible contribution to a higher rate of closure, the donut explant does not include axial mesoderm but still retains the high rate of movement of the mesendoderm observed in the whole embryo.

We asked whether a contiguous 360° of leading edge alone could increase the rate of extension of the DMZ explant. To answer this question, we placed an array of DMZ explants that would extend to form a contiguous 360° of leading edge (Fig. 10A; $n = 3$) and recorded their movements in a time-lapse sequence (Fig. 10B). Analysis of these explants shows that the leading edge begins to advance as a single DMZ explant would, but once the explants form a contiguous perimeter, the leading edge advances at a much higher rate similar to that observed in the whole embryo (Fig. 10C).

DISCUSSION

In this paper, we have resolved the movements of the mesendodermal mantle (light orange-labeled tissue in Fig. 1A) from other movements during gastrulation in the frog *X. laevis*. With the DMZ explant, we have identified protrusive activity and radial intercalation cell behaviors occurring as the mesendoderm moves away from the marginal zone during *mesendoderm extension*. Actin localizes strongly to lamellae in cells engaged in either behavior. Mesendoderm morphogenesis in DMZ explants requires interactions between the RGD and synergy sites on the FN substrate with the $\alpha_5\beta_1$ integrin receptor present on cells in the mesendoderm. We have shown that the forces driving extension of this tissue are dependent on these interactions and that propulsive forces must reside within the mesendodermal mass and not just at the clearly protrusive leading edge. In the late stages of gastrulation, once mesendoderm extension has formed the mesendodermal mantle, the mesendoderm encloses the blastocoel. During this phase of movement, the mesendoderm extends at a much higher rate than observed in the DMZ explant. Through the judicious use of explants, we have identified a geometrical requirement for the high rate of mesendodermal mantle closure seen *in vivo*. Through the use of classical embryological techniques, high-resolution imaging, and the application of integrin/FN-blocking reagents, we have identified molecular as well as physical/geometrical requirements for mesendoderm morphogenesis.

The “Hidden” Movements of Gastrulation

The early movements of gastrulation are complex and difficult to observe directly. The internal movements of gastrulation begin when a cleft is formed first on the dorsal side of the embryo after changes in cell–cell adhesion and rotational movements in the vegetal endoderm (Winklbauer and Schurfeld, 1999). Rolling movements bring mesendoderm into contact with FN fibrils (Winklbauer, 1998; Winklbauer and Schurfeld, 1999) on the blastocoelic surface of the prospective midbrain–hindbrain boundary of the neural plate (Poznanski and Keller, 1997). At the start of mesendoderm extension, anterior mesendoderm cells at the inner lip begin to ascend the underside of the animal cap

ectoderm as they gain the ability to recognize the synergy site of FN (Ramos and DeSimone, 1996; Ramos *et al.*, 1996). Once the leading edge mesendoderm contacts FN, cells begin to send out protrusions toward the animal pole as more posterior cells polarize in the more posterior mesendodermal mantle, producing shingled cell shapes, and organizing their direction of force generation. Leading edge migration and radial intercalation cell behaviors, perhaps combined with continued rolling movements in lateral and posterior sectors of the mesendoderm (Winklbauer and Schurfeld, 1999), bring the entire 360° of the mesendodermal mantle into contact with the wall of the blastocoel (Nieuwkoop and Florschütz, 1950). Forces generated by the leading edge “stretch” the more vegetal regions of the mantle. The bulk movements of the mesendoderm animalward displace the blastocoel to a more vegetal location. The mesendodermal mantle takes on a “cup-like” shape as more posterior and ventral cells move *en masse* toward the animal pole. Mesendoderm extension and formation of the mantle require the integrin $\alpha_5\beta_1$ and FN and allow a large mass of vegetal endoderm to move out of the way of the closing blastopore. As the mesendodermal mantle reaches the zenith of the animal cap, additional forces mediated by the geometry assist to drive mesendoderm mantle closure. By the end of gastrulation, the anterior and posterior edges of the mesendodermal mantle contact one another and enclose the blastocoel.

Mesendoderm cell behaviors in the DMZ explant recapitulate the cell behaviors of the mesendoderm *in vivo*. While we cannot observe mesendoderm cell behaviors *in vivo*, we have several reasons to think that cell behaviors seen in the DMZ explant recapitulate those *in vivo*. While rates of movement of the DMZ are lower than those of the whole embryo, donut or capless explants, they are similar to the rate of movement of DMZ explants that contain intact mesendoderm “lips.” Gene expression patterns also indicate that mesendoderm cells of the DMZ explant are indistinguishable from those of the whole embryo. Finally, “shingled” cell shapes and localization of actin-rich lamellae to the leading edge of cells in the DMZ explant match those seen in the whole embryo.

Dorsal Axial Convergent Extension and Mesendodermal Extension Are Mechanically Independent

Fate maps place the head mesoderm at the anterior end of the notochord; such close proximity suggests that the two are mechanically coupled and that closure of the mesendodermal mantle over the blastocoel could be accomplished either as dorsal extension pushes the head mesoderm or as the head mesoderm tows the dorsal axial tissues. The latter hypothesis was ruled out by Keller and Jansa (1992) when they demonstrated that convergent extension by dorsal mesoderm did not require traction on the underside of the animal cap. The alternative hypothesis, that dorsal axial tissue pushes the head mesoderm ahead, predicts a higher

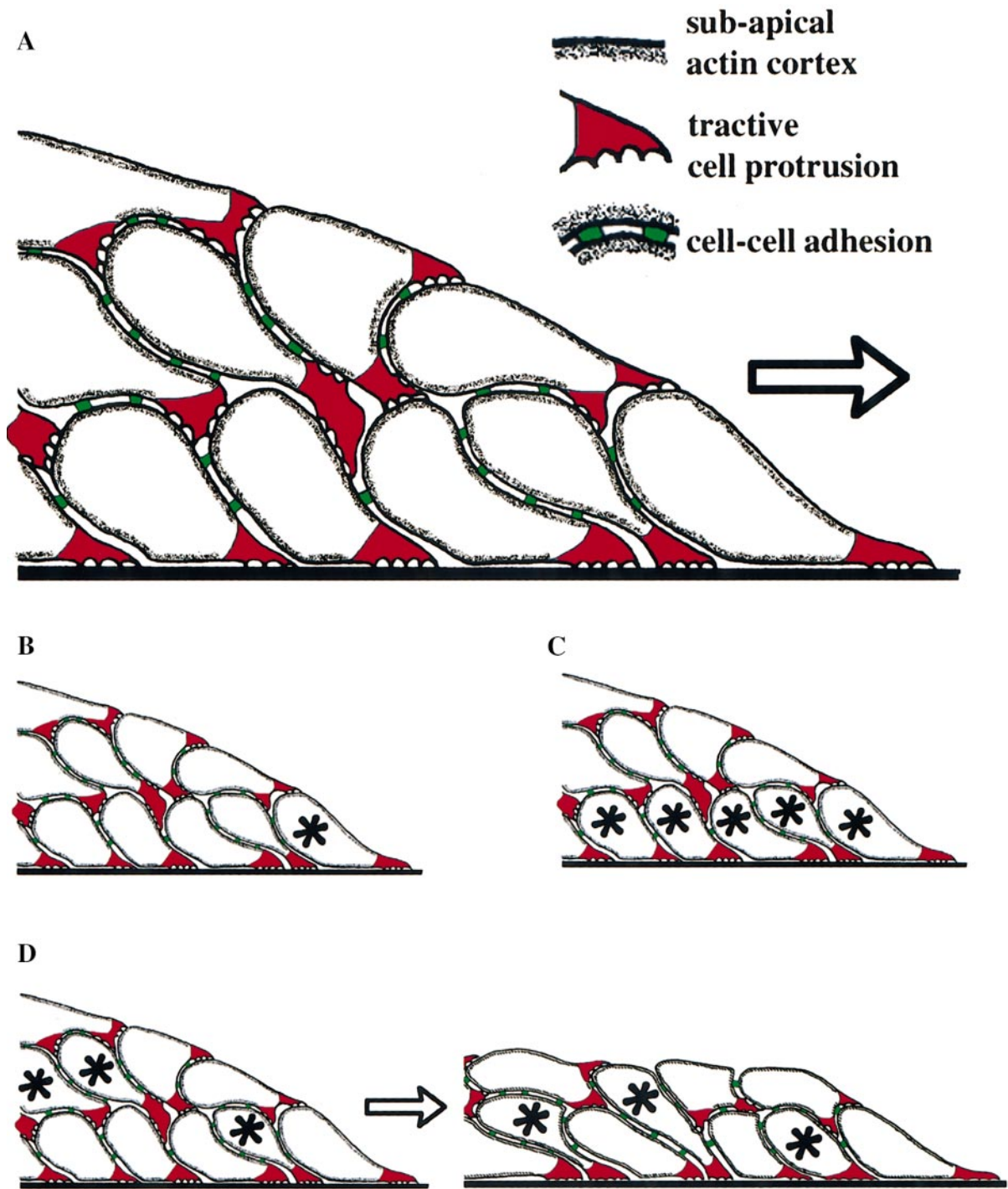


FIG. 11. Models of mesendoderm extension. (A) The mesendoderm extends as a contiguous multicell layered mass. Cells in contact with the FN-coated substrate extend tractive actin-rich protrusions at their leading edges and develop a highly polarized shingled shape. Cells within the mass also extend actin-rich protrusions as they attempt to radially intercalate. The contiguity of the mesendodermal mass is maintained by cell-cell adhesions (arrow indicates direction of movement). (B) The propulsive leading edge model proposes traction by a single row of cells at the front of the mass (asterisk) generates traction. (C) The distributed traction model proposes that all cells in contact with the substrate generate traction (asterisk). (D) The radial intercalation model proposes that cells interdigitate radially (asterisks) and then wedge between neighboring cells that are already on the substrate. These radial intercalation behaviors generate expansion forces within the mass that act to advance the leading edge.

rate of movement on the anterior side of the leading edge due to the force generated by converging and extending dorsal axial tissues. It came as a surprise to us that we could find no difference in the rate of movement between the anterior- and posterior-leading mesendoderm. Two other results, the independence of extension of the DMZ explant where extension occurs perpendicular to the dorsal axis, and the rapid closure of the mesendodermal mantle in the donut explant where the mesendoderm is microsurgically separated from the dorsal axis, provide evidence that the processes of convergent extension in the dorsal axial mesoderm and closure of the mesendodermal mantle are mechanically independent of each other.

However, convergent extension of the dorsal mesoderm may serve a redundant role ensuring mantle closure during gastrulation whenever mesendodermal extension fails. If mesendoderm extension fails, convergent extension in the dorsal mesoderm may still be capable of pushing the anterior edge of the mesendoderm over the blastocoel. Once the mesendoderm reaches a “permissive” point, cell–cell adhesion might be capable of driving mantle closure over the blastocoel. Such a backup role for convergent extension in dorsal axial tissues might explain the success of gastrulation in zebrafish or mouse mutants even when mesendodermal migration is compromised.

A Signaling Role for FN?

It has been proposed that FN has a signaling function in early embryos in addition to its role as an adhesive substrate (Marsden and DeSimone, 2001; Ramos and DeSimone, 1996; Ramos *et al.*, 1996; Winklbauer and Schurfel, 1999). From an analysis of isolated cell motility, Ramos *et al.* (1996) found that cell recognition of the RGD site was required for cell attachment. Once cells were attached, cell recognition of the synergy site was required before *Xenopus* mesendodermal cells could spread or migrate. We see analogous behavior during extension in our DMZ explants. Blocking either cell recognition of the RGD site or blocking the $\alpha_5\beta_1$ integrin causes the DMZ explant to lose its attachment to the substrate. Likewise, blocking cell recognition of the synergy site brings DMZ explant extension to a halt. Thus, “synergy” recognition appears to engage the machinery driving cell motility. The question still remaining is whether the machinery is engaged via a direct “outside-in” mechanism where attachment to RGD/synergy directly organizes the cytoskeleton or whether integrin avidity is indirectly induced after stimulation of intracellular signal transduction pathways following synergy-site recognition.

Winklbauer and coworkers (Nagel and Winklbauer, 1999; Wacker *et al.*, 1998; Winklbauer and Keller, 1996; Winklbauer *et al.*, 1992) proposed that the animal cap ectoderm produces cues localized to the fibrillar array of FN that guide dissociated mesendodermal cells and small tissue fragments toward the pole of the animal cap. However, we have determined that cues from the animal cap are not

required for directed movements in the DMZ explant or mantle closure in capless or donut explants. Our study has shown that, while such cues may exist, they are not required to guide larger more intact explants away from the dorsal axial mesoderm and bring about mantle closure under conditions where a fibrillar matrix is not present.

Biomechanical Models of Mesendodermal Extension and Blastocoel Enclosure

We have broken down the gastrulation movements of the mesendoderm into two distinct phases: the first phase in which integrin-mediated cell interactions with FN are responsible for extension of the mesendoderm leading edge along the walls of the animal cap ectoderm, and the second phase in which extension-mediating forces are joined by forces acting “in-the-round” (Figs. 8–10). Together these forces contribute to the rapid closure of the mesendodermal mantle.

Our studies suggest at least three possible models to explain mesendoderm extension in DMZ explants (Fig. 11). First, the “propulsive leading edge” model proposes that the forces driving the extension of this tissue originate solely within the leading edge itself (Fig. 11B). Leading edge cells send out actin-rich protrusions and elongate as extension proceeds, as if they were pulling out the trailing mass of the mesendoderm. This model acting alone seems unlikely because we observed that cells behind the leading edge continue to advance even when the progress of the leading edge is physically blocked. The second model (Fig. 11C), “distributed traction,” is based on the observation that cells at the leading margin as well as within the mass develop polarized actin-rich protrusions in the direction of mesendoderm extension. This model predicts that propulsive forces are generated among many contacts scattered throughout the mesendodermal mass. Similar processes can operate during wound healing (Fenteany *et al.*, 2000) when cells further back from the wound margin appear to push the margin forward. A third model for mesendoderm extension (Fig. 11D), “radial intercalation,” is based on the “vertical” interdigitation of cells within the extending explant. This model proposes that the forces driving extension result as deep cells join the single layer of cells visible at the level of the substrate (Fig. 4C). Thus, these newly added cells might act as “wedges” that push the leading edge forward from behind. In *Xenopus*, radial cell intercalation may play a role in driving numerous morphogenetic movements such as vegetal endoderm rotation that precedes mesendodermal extension (Winklbauer and Schurfel, 1999), the earliest extension movements of the dorsal axial mesoderm (Wilson and Keller, 1991), the epibolic movements of the animal cap ectoderm (Keller, 1980; Marsden and DeSimone, 2001), and neural tube formation (Davidson and Keller, 1999). However, radial intercalation does not appear to drive an increase in surface area of the extending DMZ explant, the cap-less explant, or the donut explant (bounding boxes in Figs. 4A, 8E, or 9E, respectively).

Thus, distributed traction is the most likely contributor to mesendoderm extension.

Our work identifies additional mechanisms that might assist the machinery of mesendoderm extension during the final phase of gastrulation when the mesendodermal mantle encloses the blastocoel. The first of these proposes that a “contractile purse string” draws the margin of the mesendodermal mantle closed. In a manner analogous to actin-rich purse strings seen in wound healing (Martin and Lewis, 1992) and at the margin of the epidermis in *Drosophila* dorsal closure (Edwards et al., 1997), acto-myosin structures at the leading edge could pull the margins closed. Another proposes that “forced convergence” operates in the unique geometry of the mesendodermal mantle to bring more cells into the mesendodermal mass than are necessary to expand the sheet. For instance, when the cell sheet in the DMZ explant extends by radial intercalation, the source of deep cells can become exhausted as the sheet becomes a single cell layer thick and movement of the leading edge might slow. Alternatively, a continued supply of new cells, brought about as more and more tissues are channeled into a geometrically confined space at the apex of the blastocoel roof, might enable the high rate of closure (near the point of convergence in Fig. 1B). Support for the latter model comes from our experiments to recreate the “in-the-round” conditions (Figs. 1B, 8, and 9) with multiple colliding DMZ explants (Fig. 10). Additional support for the latter model can be seen in patterns of cell rearrangement during closure of the cap-less and donut explants. As the mantle closes, cells detach from the leading edge and take up residence in the second tier of cells. This rearrangement might transiently reduce the mechanical load on the remaining leading edge cells allowing them to close faster. A more precise cellular basis for the higher rate of mesendoderm extension is the subject of another study (L.A.D. and D.W.D., manuscript in preparation).

Molecular, Cellular, and Physical Mechanisms of Mesendoderm Morphogenesis

Thinking as an engineer might, we can define *structure* as the molecular composition and cellular organization of tissues, while the term *process* can be defined as the regulation of both direction and magnitude of forces driving morphogenesis. In this paper, through the use of integrin- and FN-blocking antibodies and microsurgical techniques, we have decoupled morphogenetic machines; i.e., by isolating the morphologic *structure* from its location in the embryo we have begun to dissect the molecular role of cell-extracellular matrix adhesion in the *process*. In doing so, we have resolved tissue movements, cell behaviors, and molecular dependencies that shed light on the mechanisms that drive morphogenesis of the ventral mesoderm in vertebrate embryos.

ACKNOWLEDGMENTS

This work has been supported by the American Cancer Society (RPG93-038-06-CSM to D.W.D.) and the National Institutes of Health (USPHS/NICHHD R01-HD26402 to D.W.D. and R01-HD25594 to R.E.K.). L.D. is a Postdoctoral Fellow of the American Cancer Society. Confocal facilities provided by the W. M. Keck Center for Cellular Imaging at the University of Virginia.

REFERENCES

- Bauer, D. V., Huang, S., and Moody, S. A. (1994). The cleavage stage origin of Spemann's Organizer: Analysis of the movements of blastomere clones before and during gastrulation in *Xenopus*. *Development* **120**, 1179–1189.
- Boucaut, J. C., and Darribere, T. (1983). Fibronectin in early amphibian embryos. Migrating mesodermal cells contact fibronectin established prior to gastrulation. *Cell Tissue Res.* **234**, 135–145.
- Boucaut, J. C., Darribere, T., Boulekbache, H., and Thiery, J. P. (1984a). Prevention of gastrulation but not neurulation by antibodies to fibronectin in amphibian embryos. *Nature* **307**, 364–367.
- Boucaut, J. C., Darribere, T., Poole, T. J., Aoyama, H., Yamada, K. M., and Thiery, J. P. (1984b). Biologically active synthetic peptides as probes of embryonic development: A competitive peptide inhibitor of fibronectin function inhibits gastrulation in amphibian embryos and neural crest cell migration in avian embryos. *J. Cell Biol.* **99**, 1822–1830.
- Boucaut, J. C., Johnson, K. E., Darribere, T., Shi, D. L., Riou, J. F., Bache, H. B., and Delarue, M. (1990). Fibronectin-rich fibrillar extracellular matrix controls cell migration during amphibian gastrulation. *Int. J. Dev. Biol.* **34**, 139–147.
- Choquet, D., Felsenfeld, D. P., and Sheetz, M. P. (1997). Extracellular matrix rigidity causes strengthening of integrin-cytoskeleton linkages. *Cell* **88**, 39–48.
- Danen, E. H., Aota, S., van Kraats, A. A., Yamada, K. M., Ruiter, D. J., and van Muijen, G. N. (1995). Requirement for the synergy site for cell adhesion to fibronectin depends on the activation state of integrin alpha 5 beta 1. *J. Biol. Chem.* **270**, 21612–21618.
- Darribere, T., Guida, K., Larjava, H., Johnson, K. E., Yamada, K. M., Thiery, J. P., and Boucaut, J. C. (1990). In vivo analyses of integrin beta 1 subunit function in fibronectin matrix assembly. *J. Cell Biol.* **110**, 1813–1823.
- Darribere, T., Skalski, M., Cousin, H. L., Gaultier, A., Montmory, C., and Alfandari, D. (2000). Integrins: Regulators of embryogenesis. *Biol. Cell* **92**, 5–25.
- Darribere, T., Yamada, K. M., Johnson, K. E., and Boucaut, J. C. (1988). The 140-kDa fibronectin receptor complex is required for mesodermal cell adhesion during gastrulation in the amphibian *Pleurodeles waltlii*. *Dev. Biol.* **126**, 182–194.
- Davidson, L. A., and Keller, R. E. (1999). Neural tube closure in *Xenopus laevis* involves medial migration, directed protrusive activity, cell intercalation and convergent extension. *Development* **126**, 4547–4556.
- Dembo, M., and Wang, Y. L. (1999). Stresses at the cell-to-substrate interface during locomotion of fibroblasts. *Biophys. J.* **76**, 2307–2316.
- Domingo, C., and Keller, R. (1995). Induction of notochord cell intercalation behavior and differentiation by progressive signals in the gastrula of *Xenopus laevis*. *Development*. **121**, 3311–3321.
- Edwards, K. A., Demsky, M., Montague, R. A., Weymouth, N., and Kiehart, D. P. (1997). GFP-moesin illuminates actin cytoskeleton dynamics in living tissue and demonstrates cell shape changes during morphogenesis in *Drosophila*. *Dev. Biol.* **191**, 103–117.

- Fenteany, G., Janmey, P. A., and Stossel, T. P. (2000). Signaling pathways and cell mechanics involved in wound closure by epithelial cell sheets. *Curr. Biol.* **10**, 831–838.
- Galbraith, C. G., and Sheetz, M. P. (1999). Keratocytes pull with similar forces on their dorsal and ventral surfaces. *J. Cell Biol.* **147**, 1313–1324.
- Gurdon, J. B., Standley, H., Dyson, S., Butler, K., Langon, T., Ryan, K., Stennard, F., Shimizu, K., and Zorn, A. (1999). Single cells can sense their position in a morphogen gradient. *Development* **126**, 5309–5317.
- Kay, B. K., and Peng, H. B. (1991). "Xenopus laevis: Practical Uses in Cell and Molecular Biology." Academic Press, New York.
- Keller, R. (1991). Early embryonic development of *Xenopus laevis*. *Methods Cell Biol.* **36**, 61–113.
- Keller, R., and Jansa, S. (1992). *Xenopus* gastrulation without a blastocoel roof. *Dev. Dyn.* **195**, 162–176.
- Keller, R., and Tibbetts, P. (1989). Mediolateral cell intercalation in the dorsal, axial mesoderm of *Xenopus laevis*. *Dev. Biol.* **131**, 539–549.
- Keller, R., and Winklbauer, R. (1992). Cellular basis of amphibian gastrulation. *Curr. Top. Dev. Biol.* **27**, 39–89.
- Keller, R. E. (1978). Time-lapse cinemicrographic analysis of superficial cell behavior during and prior to gastrulation in *Xenopus laevis*. *J. Morphol.* **157**, 223–248.
- Keller, R. E. (1980). The cellular basis of epiboly: An SEM study of deep-cell rearrangement during gastrulation in *Xenopus laevis*. *J. Embryol. Exp. Morphol.* **60**, 201–234.
- Keller, R. E., Danilchik, M., Gimlich, R., and Shih, J. (1985). The function and mechanism of convergent extension during gastrulation in *Xenopus laevis*. *J. Embryol. Exp. Morphol.* **89**, 185–209.
- Kurth, T., Fesenko, I. V., Schneider, S., Munchberg, F. E., Joos, T. O., Spieker, T. P., and Hausen, P. (1999). Immunocytochemical studies of the interactions of cadherins and catenins in the early *Xenopus* embryo. *Dev. Dyn.* **215**, 155–169.
- Kushner, P. D. (1984). A library of monoclonal antibodies to Torpedo cholinergic synaptosomes. *J. Neurochem.* **43**, 775–786.
- Lane, M. C., and Sheets, M. D. (2000). Designation of the anterior/posterior axis in pregastrula *Xenopus laevis*. *Dev. Biol.* **225**, 37–58.
- Lee, G., Hynes, R., and Kirschner, M. (1984). Temporal and spatial regulation of fibronectin in early *Xenopus* development. *Cell* **36**, 729–740.
- Lo, C. M., Wang, H. B., Dembo, M., and Wang, Y. L. (2000). Cell movement is guided by the rigidity of the substrate. *Biophys. J.* **79**, 144–152.
- Marsden, M., and DeSimone, D. W. (2001). Regulation of cell polarity, radial intercalation and epiboly in *Xenopus*: Novel roles for integrin and fibronectin. *Development* **128**, 3635–3647.
- Martin, P., and Lewis, J. (1992). Actin cables and epidermal movement in embryonic wound healing. *Nature* **360**, 179–183.
- Nagel, M., and Winklbauer, R. (1999). Establishment of substratum polarity in the blastocoel roof of the *Xenopus* embryo. *Development* **126**, 1975–1984.
- Nakatsuji, N. (1975). Studies on the gastrulation of amphibian embryos: Cell movement during gastrulation in *Xenopus laevis* embryos. *Roux's Arch. Dev. Biol.* **178**, 1–14.
- Nakatsuji, N., and Johnson, K. E. (1982). Cell locomotion in vitro by *Xenopus laevis* gastrula mesodermal cells. *Cell. Motil.* **2**, 149–161.
- Nieuwkoop, P. D., and Faber, J. (1967). "Normal Tables of *Xenopus laevis* (Daudin)." Elsevier North-Holland Biomedical Press, Amsterdam.
- Nieuwkoop, P. D., and Florschütz, P. A. (1950). Quelques caractères spéciaux de la gastrulation et de la neurulation de l'oeuf de *Xenopus laevis*, Daud. et de quelques autres Anoures. *Arch. Biol.* **61**, 113–150.
- Oliver, T., Lee, J., and Jacobson, K. (1994). Forces exerted by locomoting cells. *Semin. Cell Biol.* **5**, 139–147.
- Pelham Jr., R. J., and Wang, Y. (1999). High resolution detection of mechanical forces exerted by locomoting fibroblasts on the substrate. *Mol. Biol. Cell* **10**, 935–945.
- Poznanski, A., and Keller, R. (1997). The role of planar and early vertical signaling in patterning the expression of Hoxb-1 in *Xenopus*. *Dev. Biol.* **184**, 351–366.
- Ramos, J. W., and DeSimone, D. W. (1996). *Xenopus* embryonic cell adhesion to fibronectin: position-specific activation of RGD/Synergy site-dependent migratory behavior at gastrulation. *J. Cell Biol.* **134**, 1–14.
- Ramos, J. W., Whittaker, C. A., and DeSimone, D. W. (1996). Integrin-dependent adhesive activity is spatially controlled by inductive signals at gastrulation. *Development* **122**, 2873–2883.
- Sastry, S. K., and Horwitz, A. F. (1993). Integrin cytoplasmic domains: Mediators of cytoskeletal linkages and extra- and intracellular initiated transmembrane signaling. *Curr. Opin. Cell Biol.* **5**, 819–831.
- Sater, A. K., Steinhart, R. A., and Keller, R. (1993). Induction of neuronal differentiation by planar signals in *Xenopus* embryos. *Dev. Dyn.* **197**, 268–280.
- Selchow, A., and Winklbauer, R. (1997). Structure and cytoskeletal organization of migratory mesoderm cells from the *Xenopus* gastrula. *Cell Motil. Cytoskeleton* **36**, 12–29.
- Vodicka, M. A., and Gerhart, J. C. (1995). Blastomere derivation and domains of gene expression in the Spemann Organizer of *Xenopus laevis*. *Development* **121**, 3505–3518.
- Wacker, S., Brodbeck, A., Lemaire, P., Niehrs, C., and Winklbauer, R. (1998). Patterns and control of cell motility in the *Xenopus* gastrula. *Development* **125**, 1931–1942.
- Wilson, P., and Keller, R. (1991). Cell rearrangement during gastrulation of *Xenopus*: Direct observation of cultured explants. *Development* **112**, 289–300.
- Winklbauer, R. (1990). Mesodermal cell migration during *Xenopus* gastrulation. *Dev. Biol.* **142**, 155–168.
- Winklbauer, R. (1998). Conditions for fibronectin fibril formation in the early *Xenopus* embryo. *Dev. Dyn.* **212**, 335–345.
- Winklbauer, R., and Keller, R. E. (1996). Fibronectin, mesoderm migration, and gastrulation in *Xenopus*. *Dev. Biol.* **177**, 413–426.
- Winklbauer, R., Nagel, M., Selchow, A., and Wacker, S. (1996). Mesoderm migration in the *Xenopus* gastrula. *Int. J. Dev. Biol.* **40**, 305–311.
- Winklbauer, R., and Schurfeld, M. (1999). Vegetal rotation, a new gastrulation movement involved in the internalization of the mesoderm and endoderm in *Xenopus*. *Development* **126**, 3703–3713.
- Winklbauer, R., and Selchow, A. (1992). Motile behavior and protrusive activity of migratory mesoderm cells from the *Xenopus* gastrula. *Dev. Biol.* **150**, 335–351.
- Winklbauer, R., Selchow, A., Nagel, M., and Angres, B. (1992). Cell interaction and its role in mesoderm cell migration during *Xenopus* gastrulation. *Dev. Dyn.* **195**, 290–302.
- Winklbauer, R., Selchow, A., Nagel, M., Stoltz, C., and Angres, B. (1991). Mesoderm cell migration in the *Xenopus* gastrula. In "Gastrulation: Movements, Patterns, and Molecules" (R. Keller, W. Clark, and F. Griffin, Eds.), pp. 147–168. Plenum Press, New York.

Received for publication October 10, 2001

Revised November 14, 2001

Accepted November 14, 2001

Published online January 15, 2002